UNIVERSITY OF LATVIA
FACULTY OF PHYSICS AND MATHEMATICS

Andris Fedotovs

EPR of Radiation Defects in Fluoride Crystals and in Oxyfluoride Glass Ceramics

Summary of doctoral dissertation for doctor degree in physics
Subbranch: solid state physics

Riga, 2008

The dissertation work was carried out at the Institute of Solid State Physics, University of Latvia, in the time period from year 2004 to 2008.

Type of the work: Dissertation

Scientific advisor:
Dr. habil. phys. ULDIS ROGULIS, senior researcher, Institute of Solid State Physics, University of Latvia.

Dissertation Reviewers:

1. ANDREJS SILIŅŠ; Dr. habil. phys., professor, University of Latvia,
2. JURIJS DEHTJARS; Dr. habil. phys., professor, Riga Technical University,
3. JURIS PURĀNS; Dr. habil. phys., senior researcher, Institute of Solid State Physics, University of Latvia.

The dissertation defense will take place in the open session of the Physics, astronomy and mechanics dissertation commission of the University of Latvia to be held on December 2, 2008, at 12:00 in 1st auditorium of the Institute of Solid State Physics at Ķengaraga Street 8.

The dissertation and its summary are available at the University of Latvia Library (Kalpaka Blvd. 4) and at the Latvian Academic Library (Rūpniecības Street 10).

LU Physics, astronomy and mechanics chairperson of specialized dissertation commission: emer. prof. IVARS TĀLE.

ISBN 978-9984-45-030-8

Contents

Abstract

In the present work, investigations of the structure of radiation induced defects have been performed in the BaF_2:Cd^+, $LiBaF_3$, $LiYF_4$ crystals and in the oxyfluoride glass ceramics (OxFGC) by the electron paramagnetic resonance (EPR) spectroscopy techniques.

Radiation defects in $LiBaF_3$, $LiYF_4$ crystals and in the OxFGC have been created using X-ray irradiation at room temperature (RT). The radiation defect in the BaF_2:Cd^+ crystal has been induced by γ-irradiation.

Measurements of angular dependencies of EPR spectra and obtained EPR parameters let us to explain crystallographic structure of radiation induced defects in investigated materials.

A perturbed EPR spectrum of the BaF_2:Cd^+ crystal has been explained with one nearest fluorine vacancy V_F adjacent to the Cd impurity.

In the $LiBaF_3$ crystal of high purity, the F-type centre has been observed, which EPR spectrum allowed to clarify in more details the g-tensor components and hyperfine structure (*hfs*) constants A_{Li} and A_F due to electron interaction with its nearest lithium and fluorine nuclei.

A proposed model of the radiation defect in $LiYF_4$ crystal is a F-type center, where electron has *hfs* interaction with two nearest fluorine nuclei. Our calculations with following parameters: $g_{\|} = 2.00$, $g_{\perp} = 1.975$ and $A = 27.85$ MHz are in good agreement with experimental EPR spectra of this center.

Observed *hfs* of the EPR spectra of a radiation defect in oxyfluoride glass ceramics has been explained with F-type center model in YF_3 crystalline phase. It's structure could be explained by an *hfs* interaction with it's nearest 10 fluorine and 4 yttrium nuclei.

Chapter 1

Introduction

Fluoride crystals are popular scintillation materials which could be used in the various applications of the fundamental and applied research. Therefore studies of properties of optical materials by means of various techniques of spectroscopy is still an important and actual task. Fluoride materials could be used as crystals or materials with an amorphous structure – as glasses or ceramics. They are used for the radiation detection in medical diagnostic imaging systems using X-rays or gamma rays, and in other industrial detector systems. They also find many applications in electronics, communications, etc.

The main properties of scintillators are:

1) a fast response time (10 – 100 ns),

2) a high light yield (>20000 photons per absorbed X or γ ray photon, or other particle, e.g. neutron),

3) a high density ρ, and high atomic number Z, for efficient gamma ray detection.

There are good points and also some drawbacks for each particular kind of scintillators. The ideal scintillator material has not been synthesized yet. Therefore the most suitable material should be considered for every specific application, basing on its physical and chemical properties and on other requirements, such as costs and peculiarities of production. For example, such materials as NaI:Tl, CsI:Tl, CsI:Na, $CdWO_4$ have light yields $\geq 10^4$ photons/MeV, but decay times are too large $>$200 ns. In contrast, BaF_2, CsF, CeF_3, CsI have decay times in the range $\sim 1-30$ ns, but their light yield is as low as only $\sim 10^3$ photons/MeV [1].

Besides the properties of the material *per se*, considerable role belongs to the defects in the crystals. The defects could appear in an any stage of the materials life. They could be created during the crystal growth or during its exploitation, when the material is exposed to the extreme chemical and intense ionizing radiation conditions. As a consequence structural defects such as dislocations or interstitials could be created, which, in principle, could cause definite deformation of the material. Other types of defects are intrinsic defects or so called *point defects*, which are stoichiometric irregularities of interatomic range. Hereafter, in this work, only point defects induced by the ionizing irradiation will be considered.

Intrinsic defects introduce notable changes in the electronic energy level structure of materials causing their own energy levels and bands to appear. These bands could be used for various applications, for example, rare-earth impurities are a fundamental part of many laser active media. However, often such defect bands could be cumbersome.

For the complete understanding of the structure of a particular defect in the material, its electronic and crystallographic structure should be investigated.

Methods of the magnetic resonance are structure sensitive methods and are especially suited for studies of crystallographic structure of the defects, since it is possible to measure the interaction of electron spin with magnetic moments of its nearest surrounding nuclei. Electron paramagnetic resonance (EPR) is one of the most widely used magnetic resonance methods.

The current work is a summary of EPR studies of irradiation induced defects in the fluoride crystals and in oxyfluoride glass-ceramics.

1.1 Motivation

Investigated crystals BaF_2, $LiBaF_3$ un $LiYF_4$ are popular scintillation materials in the fields that use detection of high-energy radiation [1–3]. These crystals possess very good scintillator properties, however, these properties could be diminished by various uncontrolled impurities which could cause structural inhomogeneities and forming of the color centers in the crystal matrix.

A growing interest on optical composite materials has been raised recently. These are glass-ceramics composites with nanosized crystallites incorporated in the glass matrix.

What concerns the defects in these materials, the purity of the ingredients is a very important aspect. Uncontrolled impurities could cause unwanted spectral luminescence and absorbtion bands in specific optical range. For example, in the case of fluorides, a common impurity defect is oxygen, which penetrates in the material during the crystal growth, some another fluoride compound should be used to bond and evaporate the oxygen from the hot melt.

1.2 The aim of the work

The aim of this work is to investigate structure of radiation defects in aforementioned fluoride crystal scintillator materials and in oxyfluoride glass-ceramics. The following tasks have been set:

1. To obtain the experimental EPR spectra set in the BaF_2:Cd^+, $LiBaF_3$, $LiYF_4$ crystals and in the oxyfluoride glass ceramics (OxFGC) after exposing them by the ionizing irradiation.
2. To determine EPR parameters of induced radiation defects.
3. To analyse reasonable models of the paramagnetic centers.

Author's contribution

The work in its entirety has been done in the Institute of Solid State Physics of University of Latvia. All EPR experimental measurements and theoretical analysis have been performed by the author. Theoretical analysis and calculations have been done using specific computer software.

Novelty of the work

Experimental investigations of this work have let to identify new radiation defects in significant scintillation materials – fluoride crystals and oxyfluoride glass ceramics. The obtained EPR parameters from the spectra allow to describe and propose models for the structure of the radiation induced defects. The results could be used for the further studies of these materials and also for other fluoride-based materials in order to improve their properties.

Chapter 2

EPR spectroscopy

EPR is a field of spectroscopy, which investigates transitions between electron Zeeman levels which appear in the external magnetic field. Similarly as in the optical spectroscopy, EPR spectra are absorption spectra. The difference is, that the EPR transitions occur in the microwave range of the electromagnetic waves.

EPR spectrum could be described with three main groups of parameters:

1) Fine structure parameters (spin-orbital and crystal field effects),

2) g-factor (electron Zeeman interaction),

3) Hyperfine (hf) parameters, which describe interaction of unpaired electron spin with nuclear magnetic moments.

External magnetic field causes splitting of electron spin levels. Transition energy between these levels is equal to microwave energy, emitted by a klystron. The condition of the resonance is a following relationship between the microwave quantum $h\nu$ and the energy difference between the Zeeman levels of an electron $g\beta B$:

$$h\nu = g\beta B \tag{2.1}$$

where h – is the Plank's constant, ν – frequency, g – a spectroscopic splitting factor, where an atomic spin-orbital contribution is taken into account, β – Bohr magneton, B – magnetic field.

This relationship shows that:

1) magnetic field B induces a Zeeman field splitting and determines the transition energy,

2) microwave quantum $h\nu$ induces a spin transition from lower energy state to upper state, causing the absorption line,

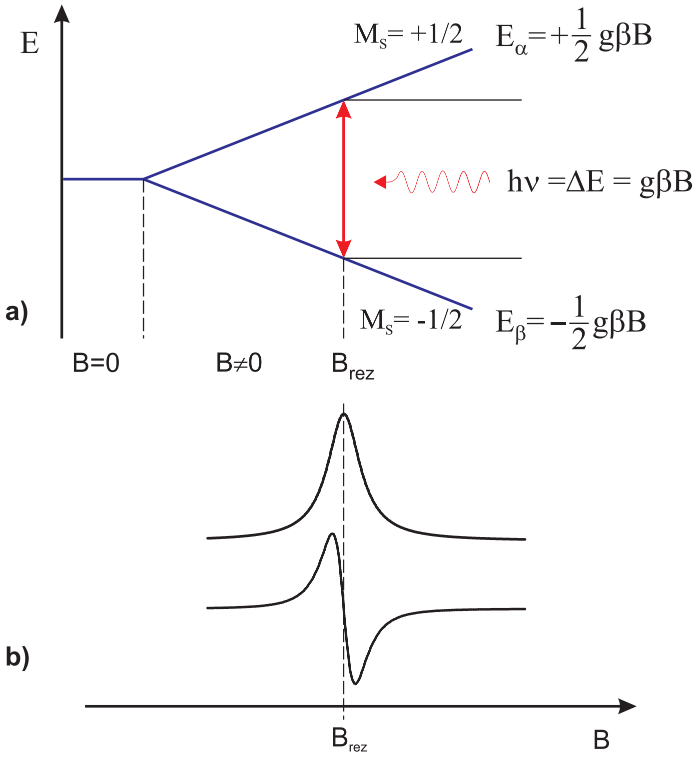

Figure 2.1. *Zeeman effect and EPR transition with absorption of the microwave quantum, if the magnetic field has reached the resonance value.*

3) g-factor determines the position of the absorption line in the EPR spectrum. It depends of the paramagnetic electron state in the solid.

2.1 Spin - Hamiltonian parameters

All interactions of the paramagnetic resonance could be described using the following spin Hamiltonian:

$$\mathscr{H} = \hat{H}_0 + \underbrace{\beta \mathbf{S}\hat{g}\mathbf{B}}_{\hat{H}_{EZ}} + \underbrace{\mathbf{S}\hat{D}\mathbf{S}}_{\hat{H}_{SS}} + \underbrace{\mathbf{I}\hat{A}\mathbf{S}}_{\hat{H}_{hss}} + \underbrace{\mathbf{I}\hat{Q}\mathbf{I}}_{\hat{H}_{Q}} + \underbrace{\beta_N \mathbf{I} g_N \mathbf{B}}_{\hat{H}_{KZ}} \tag{2.2}$$

Each term in the spin Hamiltonian determines a specific interaction of the electron and nuclear magnetic moments in the discussed energy range:

1) $\hat{H}_{EZ}$ – electron Zeeman interaction,

2) $\hat{H}_{SS}$ – electron fine structure interaction,

3) $\hat{H}_{HSS}$ – electron-nuclear hyperfine interaction,
4) $\hat{H}_Q$ – nuclear quadrupole interaction,
5) $\hat{H}_{KZ}$ – nuclear Zeeman interaction.

Other symbols in the spin Hamiltonian terms have the following meaning:

- β – Bohr magneton;
- **S** – electron spin operator;
- $\hat{g}$ – g-factor operator, which is a general case is a tensor;
- **B** – magnetic field intensity;
- $\hat{D}$ – crystal field (fine structure) interaction tensor;
- **I** – nuclear spin operator;
- $\hat{A}$ – hyperfine interaction tensor.

The g-factor, which is a part of the resonance condition (2.1), defines the position of the absorption lines in the EPR spectrum. Generally, g-factor is described by a diagonal tensor and contains following components, depending on the crystal field symmetry:

1) cubic — g,
2) axial — $g_{||}$ un $g_{\perp}$,
3) orthorhombic — g_{xx}, g_{yy} un g_{zz}.

In such case an effective value of the g-factor could be used. For axial symmetry it is expressed as

$$g_{eff}^2 = g_{||}^2 \cos^2\theta + g_{\perp}^2 \sin^2\theta \tag{2.3}$$

where θ is the angle between magnetic field **B** direction and the symmetry axis of the defect [4].

2.2 Hyperfine structure of the EPR spectra

The third term $\hat{H}_{HFS}$ of the previously described spin Hamiltonian is the most important term, what helps to interpret the EPR spectra. This term describes an interaction of the unpaired electron spin with the spins of the nearest nuclei, the so called hyperfine (*hf*) interaction. In case of the EPR *hf* structure, these spectra contains the most useful information about the paramagnetic center.

From the classical point of view, the hyperfine interaction could be described as a dipole-dipole interaction of the electron and nuclear magnetic moments (see figure 2.2) with the following energy:

$$W_{dip} = \frac{\mu_e \cdot \mu_N}{r^3} - \frac{3(\mu_e \cdot \mathbf{r})(\mu_N \cdot \mathbf{r})}{r^5} \tag{2.4}$$

where $\mathbf{r}$ is the vector of the distance connecting both dipoles, μ_e and μ_N – magnetic moments of the electron and nucleus, respectively [4]. By replacing of the magnetic moments to the corresponding operators, the Schrodinger's equation could be written in the following form:

$$\hat{H}_{dip} = -g\beta g_N \beta_N \left[\frac{\hat{\mathbf{S}} \cdot \hat{\mathbf{I}}}{r^3} - \frac{3(\hat{\mathbf{S}} \cdot \mathbf{r})(\hat{\mathbf{I}} \cdot \mathbf{r})}{r^5} \right] \tag{2.5}$$

If the spin operators are written by their spatial components, it could be seen that the dipole interaction includes an interaction between tensors, what means that the result could be dependent on the direction of the hyperfine interaction. Such systems are called *anisotropic*. For the spin system with the electron spin $S = 1/2$ and nuclear spin $I = 1/2$, the spin Hamiltonian is

$$\hat{\mathscr{H}} = \beta \hat{\mathbf{S}} \cdot \hat{g} \cdot \mathbf{B} + h\hat{\mathbf{S}} \cdot \hat{A} \cdot \hat{\mathbf{I}} - g_N \beta_N \mathbf{B} \cdot \hat{\mathbf{I}} \tag{2.6}$$

If unpaired electron has an hyperfine interaction with multiple neighboring nuclei, then the *hf* interaction with each specific nuclei should be accounted:

$$\hat{\mathscr{H}} = \beta \hat{\mathbf{S}} \cdot \hat{g} \cdot \mathbf{B} + \sum_i^n \left(h\hat{\mathbf{S}} \cdot \hat{A}_i \cdot \hat{\mathbf{I}}_i - g_{N_i} \beta_{N_i} \mathbf{B} \cdot \hat{\mathbf{I}}_i \right) \tag{2.7}$$

The selection rules for the EPR hyperfine transitions are $\Delta M_S = \pm 1$ and $\Delta M_I = 0$, as it could be seen in figure 2.3. If the paramagnetic center has n neighboring nuclei with $I = 1/2$, then the number of allowed transitions is

$$N = (2 \cdot I + 1)^n \tag{2.8}$$

Usually the hyperfine interaction constant A is expressed in megahertz or in militeslas. It determines the hyperfine interaction energy between the electron and nucleus. It could

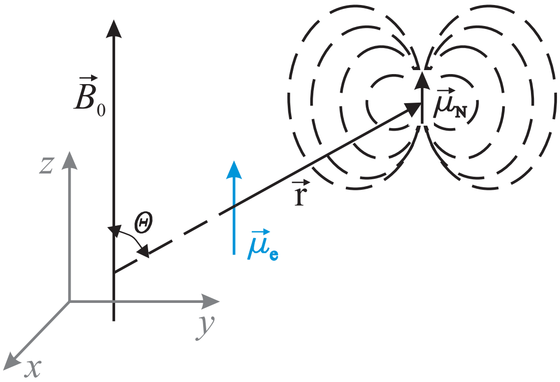

Figure 2.2. *The hyperfine interaction of the electron and nuclear spins.*

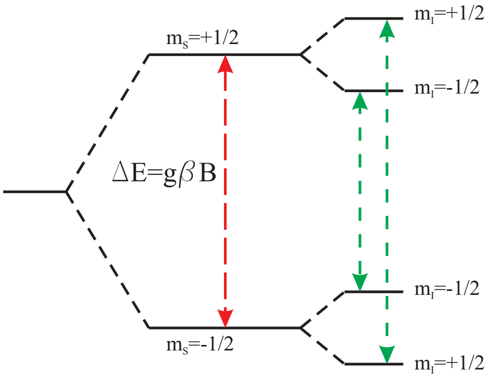

Figure 2.3. *Hyperfine splitting of the Zeeman levels in case of the nuclear spin I=1/2.*

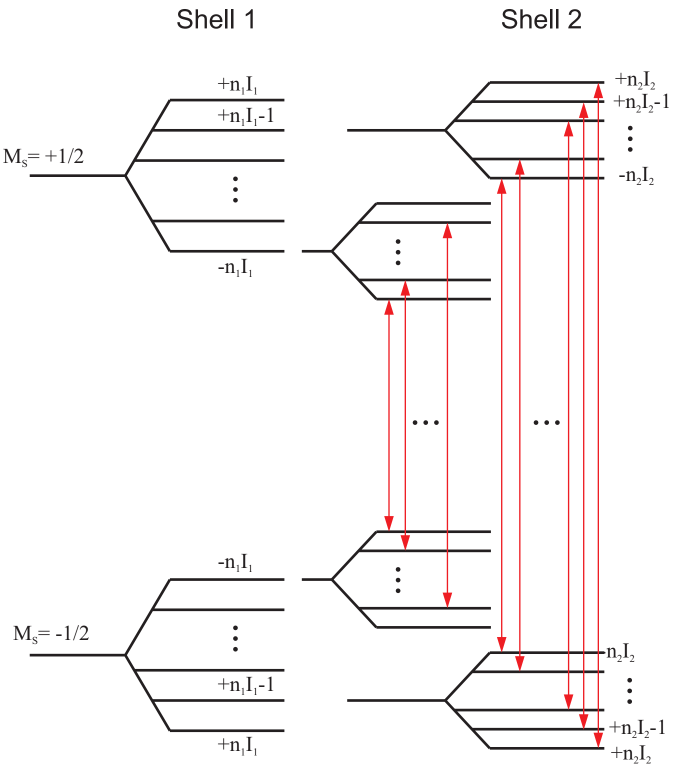

Figure 2.4. *Energy level scheme for an electron S=1/2 with hyperfine coupling to several shells of equivalent nuclei with spins I_1 and I_2.*

be different for various crystallographic directions. In such cases, the hyperfine constant is expressed as a diagonal tensor:

$$\hat{A} = \begin{pmatrix} A_{xx} & 0 & 0 \\ 0 & A_{yy} & 0 \\ 0 & 0 & A_{zz} \end{pmatrix} \tag{2.9}$$

If the paramagnetic center possess an axial symmetry, the magnetic field could be oriented along one of the main crystallographic directions [100], [110] or [111] during the experiment. In this case, the hyperfine interaction tensor could be written as follows:

$$\hat{A} = \begin{pmatrix} A_{\perp} & 0 & 0 \\ 0 & A_{\perp} & 0 \\ 0 & 0 & A_{\parallel} \end{pmatrix} \tag{2.10}$$

where $A_{\perp}$ – is the value of the hyperfine interaction tensor component, which is perpendicular to the magnetic field, and $A_{\parallel}$ – component, which is parallel to the magnetic field. Effective value A for other orientations could be estimated as follows:

$$A_{eff}^2 = A_{\parallel}^2 \cos^2\theta + A_{\perp}^2 \sin^2\theta \tag{2.11}$$

The hyperfine interaction tensor could be also expressed as a sum of its isotropic part a and anisotropic part b:

$$a + \begin{pmatrix} -b & 0 & 0 \\ 0 & -b & 0 \\ 0 & 0 & -2b \end{pmatrix} = \begin{pmatrix} A_{\perp} & 0 & 0 \\ 0 & A_{\perp} & 0 \\ 0 & 0 & A_{\parallel} \end{pmatrix} \tag{2.12}$$

or $A_{\parallel} = a + 2b$ and $A_{\perp} = a - b$ [4].

2.3 Interpretation of the EPR spectra

Basic information which could be obtained from the EPR spectra consists of number of spectral lines and their intensity distribution, which is determined by the number and type of the spins involved in this center. The value of the hyperfine constant could be directly estimated from the distance between the hyperfine lines in the EPR spectra.

Generally n nuclear spins with spin I give $k = 2nI + 1$ lines in the spectrum. If the system consists of nuclei with different spins, then the number of lines could be determined by the following expression:

$$n = \prod_i (2n_i I_i + 1) \tag{2.13}$$

where n_i -– number of specific nuclei [4].

	n
1	**0**
1 1	**1**
1 2 1	**2**
1 3 3 1	**3**
1 4 6 4 1	**4**
1 5 10 10 5 1	**5**
1 6 15 20 15 6 1	**6**
1 7 21 35 35 21 7 1	**7**

Figure 2.5. *Binomial distribution of intensities of superhyperfine lines of EPR spectra in dependence of a number of nuclei* n *with spin I=1/2.*

Since the transitions between hyperfine energy levels, according to the selection rules, occur only between levels with equal M_I, it is easy to see that intensities of the hyperfine lines in the resulting EPR spectrum should have a binomial distribution, as it is seen in the figure 2.5. Intensities of the lines are dependent on the number of transitions in the specific energy range, thus the resulting spectrum could be interpreted as the superposition of all possible transitions in the spectra. the energy level splitting scheme for the electron spin of $S = 1/2$ is shown in figure 2.4.

Chapter 3

Studies of radiation defects

Studies of the ionizing radiation impact on the materials is one of the fundamental fields of contemporary science. Various structural changes could occur in the material during interaction with high energy radiation, which are not always desirable. Thus it is important to predict what could happen in the material, if it is exposed in extreme ionizing environment for the prolonged period of time. Especially important it is in the case of crystalline and ceramic substances, which are common materials used as scintillators in the radiation detection devices and as laser active media. Crystals, currently investigated in this work, find broad applications in these fields, and in the next subsections a brief summary about radiation defects in these crystals will be given.

During radiation interaction with the matter, a part of its energy goes to the excitation of the electronic subsystem. This part of energy plays crucial role in the process of the point defect formation. That mechanism became clear, when a coloration of the wide band-gap materials had been observed. Color centers or "F-centers" in the material are formed during a soft X-ray irradiation (10-100 keV range). F-center is an electron localized in the anion vacancy (see figure 3.1). Mechanisms of creation of these centers have been studied already fifty years ago [5].

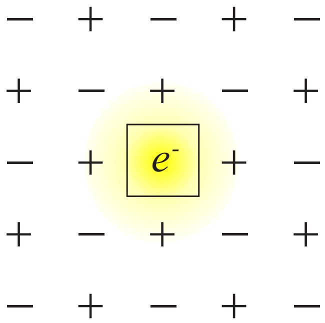

Figure 3.1. *Structure of the F-type center in the alkali halide crystals.*

3.1 in the BaF$_2$ crystals

Cadmium impurity defect in BaF$_2$ crystals has been studied by means of optical and magnetic resonance methods [6–9]. In the work [6], EPR parameters of the *regular* Cd$^+$ impurity center in the CaF$_2$, SrF$_2$ and BaF$_2$ crystal matrixes have been determined. In this configuration, cadmium ion Cd^{2+} replaces a cation and thus has eight fluorine ligands in its nearest surrounding. An electron is captured on the cadmium impurity, after X-irradiation at room temperature. It's state is $^2S_{1/2}$. Judging from the EPR spectra, the electron has a strong hyperfine interaction with its nearest fluorine ligands, which has a nuclear spin $I = 1/2$. The EPR spectrum of this center consists of 9 lines with binomially distributed intensities. Also a formation of the V$_K$ centers had been observed after irradiation of the sample at low temperatures.

A corresponding spin Hamiltonian for the Cd$^+$ center in the BaF$_2$ crystal could be written as follows:

$$\hat{\mathscr{H}} = g\beta B\hat{S} + SA^{Cd}I^{Cd} + \sum_i \left(SA_i^F I_i^F\right) \tag{3.1}$$

where g is a g-factor of the Cd$^+$ center, β – Bohr magneton, B – magnetic field intensity, S – electronic spin, A^{Cd} – hyperfine interaction constant for the Cd nuclei, $I^{Cd} = 1/2$ nuclear spins of odd Cd isotopes ^{111}Cd and ^{113}Cd (^{112}Cd nuclear spin I=0). Hyperfine EPR spectra of odd cadmium isotopes are comparably weak due to their low natural abundancies (12.75% for ^{111}Cd and 12.26% for ^{113}Cd respectively). Moreover the *hf* spectra of these species are overlapped and therefore could not be well resolved. The third term in the spin Hamiltonian (3.1) accounts a hyperfine interaction $A_i^F I_i^F$ of the every surrounding fluorine ligand with the electron spin S.

The Cd$^+$ ions is located in the field of cubic symmetry, and could cause axial deformations of the field towards every fluorine ligand (see figure 3.2). These deformation axis coincide with the diagonals of the cube.

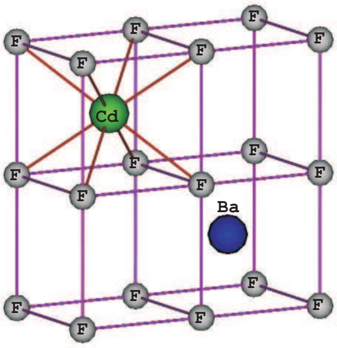

Figure 3.2. *Structure of the regular Cd$^+$ impurity defect in the BaF$_2$ crystal.*

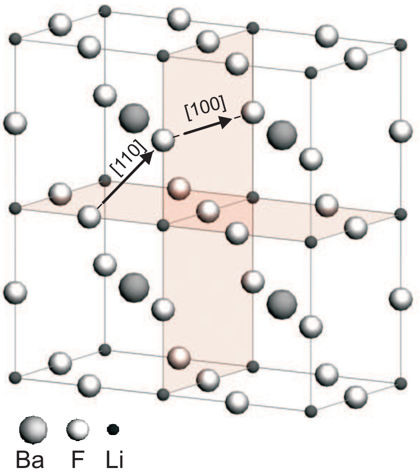

Figure 3.3. *Crystallographic structure of the LiBaF$_3$ crystal.*

3.2 in the LiBaF$_3$ crystals

LiBaF$_3$ crystals possess antiperovskite crystallographic structure (see figure 3.3). Investigations of the radiation defects in these crystals have been done recently. V$_K$ type centers (localized hole) after irradiation at low temperatures has been observed. Several optical absorbtion bands characteristic to F-type centers have been observed after sample X-irradiation at room temperature. For the first time EPR spectrum of the F-center in the LiBaF$_3$ has been detected in the samples doped with Fe impurity [10]. Main drawback of these investigations was a broad absorbtion line which partially obscured EPR spectra of the F-type center. Other type of measurements in the pure LiBaF$_3$ crystal were done by means of optically detected EPR method, which is based on the excitation of the recombination luminiscence (RL-EPR). Measurements of the magnetic circular dichroism of the optical absorbtion (MCDA) and MCDA detected EPR of the X-irradiated crystal showed a presence of F-type center in the lattice with explicit g-factor anisotropy. However, these measurements have not revealed important information about the *hf* interaction nature of this center.

In order to explain the angular dependencies of the RL-EPR spectra, the following spin Hamiltonian had been used:

$$\hat{\mathscr{H}} = \mu_B \cdot \mathbf{B} \cdot \hat{g} \cdot \mathbf{S} \tag{3.2}$$

assuming $S = 1/2$ and an axial g-tensor with its main axis along the [100] direction.

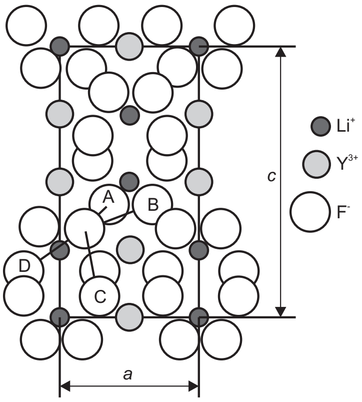

Figure 3.4. *Projection of the unit cell of the* LiYF$_4$ *on to the* ac *plane [18].*

3.3 in the LiYF$_4$ crystals

LiYF$_4$ crystals are widely used as scintillators and as laser active media materials [1, 11, 12]. Due to their good capability to host trivalent rare earth elements such as Nd^{3+}, Dy^{3+}, Er^{3+}, Yb^{3+}, Ce^{3+}, these crystals provide a popular material for doping with rare earth ions, since replacing Y^{3+} by the mentioned ions does not need additional charge compensation [13–15].

Recent studies on this subject cover a wide range of optical and magnetic properties in doped and pure LiYF$_4$ crystals [13–22]. Authors of [17, 18] report on the details of radiation defects induced by X-ray irradiation at 77 K in the pure LiYF$_4$ crystal.

The most common center generated under such irradiation is the V$_K$ (F$_2^-$) center. Elaborated studies of this type of center in LiYF$_4$ were carried out in [19]. EPR spectra of such a center consist of four lines caused by the hyperfine interaction of two neighboring fluorine nuclei with a self-trapped hole. The structure of this center in the LiYF$_4$ is similar to those in other halides. However, there are four possible kinds of V$_K$ centers in the LiYF$_4$. None of these possible V$_K$ centers are thermally stable, i.e., they have comparatively short living time even at low temperatures, e.g., the most stable V$_K$ center relaxes after 60 min. at 77 K, with a glow peak at 75 K [17–19]. The structure of the LiYF$_4$ lattice is shown in the figure 3.4.

Another most common defect in inorganic halide crystals is the F-type center, which is a halide ion vacancy with a trapped electron. As a possible model for such center in a LiYF$_4$ crystal the authors of [17] proposed a defect with the dipole alignment along the Y^{3+}-Y^{3+} ion direction.

However, there are no experimental data for such model done by structure–sensitive magnetic resonance methods like EPR. In the optical absorbtion and luminscence measurements characteristic spectra at 331 nm of V$_K$ center had been observed [20]. Additional unidentified spectral bands peaking at 411, 431 and 542 nm were observed. A stimulated emission effect has been detected by exciting some of the color centers [20].

3.4 in oxyfluoride-glass ceramics (OxFGC)

Oxyfluoride glass ceramics are novel materials which posses promising optical and mechanical properties. New glass ceramics materials have been obtained at the Institute of Solid State Physics, University of Latvia [23]. These materials find a broad application in various fields. Basing on the glass ceramics, active media of lasers and also scintillators could be produced. Thus, investigations of the optical properties for these materials are important. Most of the intrinsic and impurity defects affects optical properties of the matter. Many recent investigations in glass-ceramics materials concerns rare earth element impurities Er^{3+} [24–29], Nd^{3+}, Pr^{3+}, Yb^{3+}, Ho^{3+} [30, 31]. Energy transfer between rare earth energy levels provide the so-called *up-conversion* process. Recent investigations show that in the glass-ceramics materials this process is even more efficient than in single crystals [24, 29]. There are numerous studies of luminescence and optical absorbtion in these materials, however, studies concerning paramagnetic properties of radiation induced intrinsic defects are rare. Since the glass ceramics materials are promising in the detection and transforming of high energy radiation, it is critical to know and predict their stability under such conditions.

Main feature of the glass ceramics is that part of the material have been crystallized, containing crystalline phases as nanosized particles. As host materials basically SiO_2, B_2O_3 or P_2O_5 are used. Oxyfluoride glass is synthesized by adding fluoride components to the raw material. OxFGC synthesis consists of two phases: 1) the growth of the particular glass; 2) the glass-ceramics creation using thermal treatment at specific temperatures. During a specific heat treatment, fluoride compounds could form crystalline structures. It is possible, because fluorides are chemically principally different class and do not bond well with the host oxide material. As a result, nanosized crystallites are formed into the glass matrix. Their sizes could range from 8 – 25 nm. OxFGC possess such features as high thermal and chemical stability and notably higher mechanical endurance as the corresponding crystalline materials.

As already mentioned, EPR studies in these materials are rare due to the disordered structure of the glass ceramics. Thus it is reasonable to compare the EPR spectra in the single crystals and spectral properties of the EPR in glass ceramics. In case of OxFGC the information previously observed about fluoride crystals BaF_2, $LiBaF_3$, LiF and $LiYF_4$, could be used for the EPR analysis. However, some crystals could have more than one crystallographic structure. For example, it is known that besides it's normal – scheelite structure, the $LiYF_4$ crystals could possess other types of structures as well [32]. Similar situation is with the YF_3 crystal, which is difficult to obtain as single crystals [33]. Thus such glass ceramics with incorporated YF_3 crystallites could be an excellent alternative to the YF_3 single crystals.

Chapter 4

Experimental

4.1 EPR spectrometer

For microwave absorbtion measurements in the system with unpaired electronic magnetic moments – spins, one should use a spectrometer with a permanent, linearly adjustable magnetic field.

A standard EPR spectrometer consists of four blocks:

1) *A microwave source unit*, which provides a monochromatic radiation at a specific frequency and adjustable intensity, and also serves for detection of transmitted radiation.

2) *An electromagnet system* provides stable and homogenous, linearly controllable magnetic field.

3) *A resonator system* consist of a resonator, where the sample is placed during the experiment, and microwave guides to track the source radiation to the sample and back to the detectors.

4) *A detection unit* senses the EPR absorbtion signal, filters and amplifies it.

To obtain the EPR spectra, we used a standard EPR spectrometer РЭ-1306. This particular model is suited for EPR measurements in the so called X-band range, with a characteristic frequency of $\sim$9.5 GHz. The wavelength of this radiation is $\sim$3 cm. The magnetic field is in the 100 – 7000 Gs range. The precision of the magnetic field scan is 0.5 Gs. The external magnetic field is modulated by adding a perpendicular component of the alternating field, provided by small coils in the resonator. A typical modulation frequency is 100 kHz. Thus, the first derivative of the absorbtion line is recorded. The block diagram of the EPR spectrometer is shown in the figure 4.1.

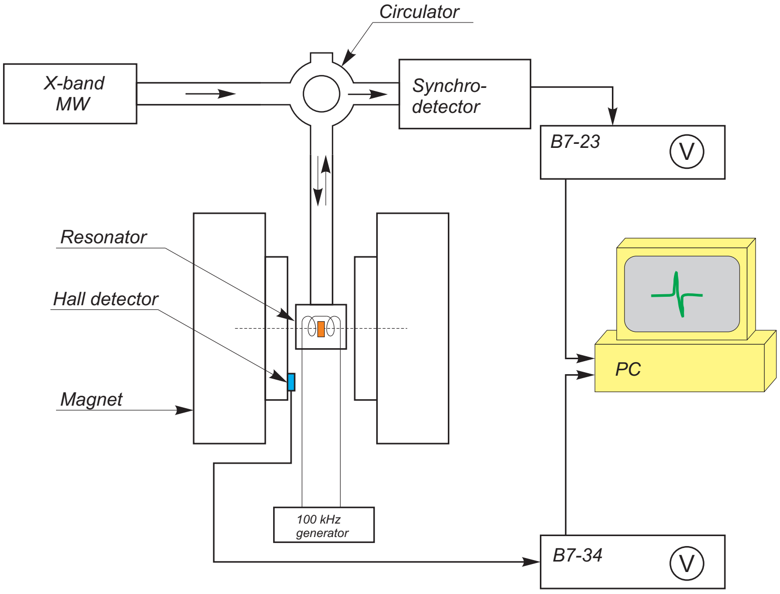

Figure 4.1. *A block diagram of the EPR spectrometer* РЭ-1306.

4.1.1 Magnetic field modulation

Usually, the transmitted EPR signal is accompanied by various noise components. For improvement of the signal-to-noise ratio, lock-in amplification techniques have to be used. For this purpose, the static magnetic field B_0 is modulated at a specific frequency. As a result, an alternating current with the modulation frequency is detected. This signal is easy to amplify with a lock-in amplifier. A frequency band of 100 kHz is commonly used for the modulation. It is realized by placing small coils on the axes of the external magnet. If the amplitude of modulation is comparably small, then the amplitude of the 100 kHz signal will be proportional to the inclination of the absorbtion line in the center of the modulation field (see 4.2). It could be seen that it will have a maximum at the halfwidth of the absorbtion line, but will be equal to zero at the peak point of absorbtion line. Thus, a first derivative of the absorbtion line is detected. A typical power of the microwave radiation is approximately 1 mW, and a heterodyne detection system is used for measurements of such a weak radiation.

4.1.2 X-ray irradiation

The X-irradiation power supply unit provides max. 20 mA current at 60 kV voltage. We used X-ray tubes of type БСВ2-W with a tungsten as anode material. A typical irradiation voltage was ~50 kV with 10 mA current, usually for 30 min – 1 h long periods of time.

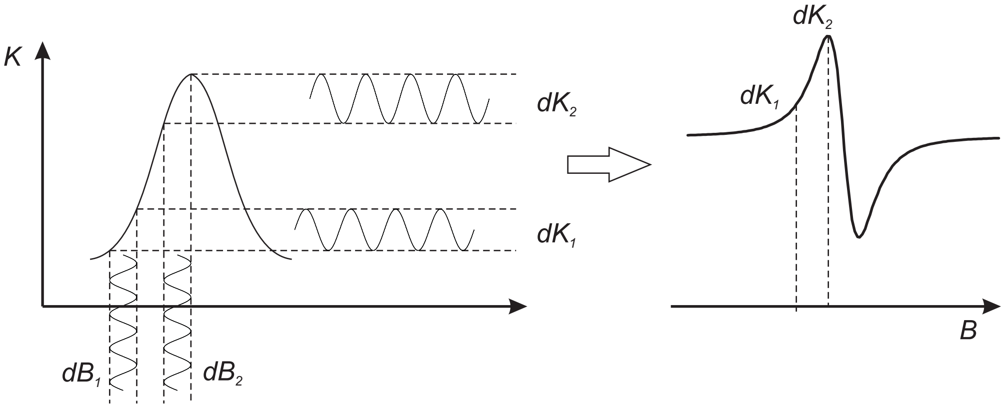

Figure 4.2. *Magnetic field modulation and absorbtion line detection.*

4.2 Investigated samples

Experimentally investigated samples of the BaF_2:Cd^+, $LiYF_4$ crystals and OxFGC have been grown at the Institute of Solid State Physics of University of Latvia (A. Veispāls, L. Dimitročenko). The $LiBaF_3$ crystal of high purity degree has been grown at the Waseda University, Japan (N. Ichinose, K. Shimamura). All crystalline samples were oriented, in order to identify relevant crystallographic directions. EPR angular measurements have been done by orientation of the magnetic field in the specific crystallographic plane. The EPR measurements for the $LiBaF_3$, $LiYF_4$ and OxFGC were done at liquid nitrogen temperatures – 77 K. The EPR measurements of the BaF_2:Cd^+ were done at room temperature. Measurements at low temperatures were done by using of a glass dewar, which was filled with liquid nitrogen, in which the sample mounted on the quartz sampleholder was immersed.

BaF_2:Cd^+

This crystal has been grown in the vacuum with approx. cadmium concentration of 0.02 at.%. Sample was irradiated with γ-rays at room temperature. Measurements of the EPR angular dependencies were carried out at RT in the (110) plane, changing magnetic field orientation from [100] direction to [110] with an increment of 5°.

$LiBaF_3$

This sample has been grown with a high degree of purity, without any dopants. The orientation of crystallographic axis was done, and EPR measurements were carried out in the (110) plane rotating from [100] to [110] direction at 77 K. The X-irradiation was done at RT.

$\mathbf{LiYF_4}$

The $LiYF_4$ crystal has a tetragonal scheelite structure. It's symmetry group is $I4_1/a$, which is homologous to the well-known $CaWO_4$ structure. The lattice constants are $a = b = 5.26$ Å and $c = 10.94$ Å. Each Li^+ ion is tightly bounded within a regular fluorine tetrahedra, and each Y^{3+} ion is surrounded by eight fluorines, which forms a tetragonal dodecahedron [15]. The optical axes of the crystal have been determined by means of optical polarization microscope. The X-irradiation was done at RT. Measurements of the EPR angular dependencies were carried out in two planes: 1) rotating magnetic field from $\mathbf{b} \parallel c$ to $\mathbf{B} \perp c$ and 2) rotating crystal around the fourfold axis c, thus orientating the magnetic field in the plane *ab*. The EPR measurements were performed at 77 K.

OxFGC

The OxFGC has been synthesized from the following ingredients: 50 mol% SiO_2, 25 mol% Li_2CO_3, 20 mol% YF_3, 3 mol% YbF_3 and 2 mol% ErF_3. The obtained glass sample was then treated in heat at 555°C temperature for 20 minutes, till the ceramics phase was formed. Both samples – glass and glass-ceramics were X-irradiated at RT. EPR measurements were performed at 77 K.

4.3 Analysis of EPR spectra

One of the most important phases of the EPR spectral analysis is a theoretical simulation of the spectra using spin Hamiltonian parameters of the specific paramagnetic center. The precision of the calculated spectra depends on the applied approximation and matrix diagonalization methods [34].

One of the simplest approximation methods is a mathematical calculation of the EPR transition lines positions in the spectrum. As the next step, the appropriate function, characteristic to the absorption line is fitted. Usually this is either Lorentz or Gaussian type function. From the chapter 2, the spin Hamiltonian of the paramagnetic center, which describes the electron Zeeman interaction and hyperfine interaction with nearest n neighbors with the nuclear spin I is:

$$\hat{\mathscr{H}} = g\beta B\hat{S} + \sum_{i}^{n} A_i \hat{S} \cdot \hat{I}_i \tag{4.1}$$

This particular system contains spins with following values:

$$|M_S; M_{I_1}, M_{I_2}, \ldots, M_{I_n}\rangle \tag{4.2}$$

whose energies are expressed by the relationship:

$$E(M_S, M_{I_1}, M_{I_2}, \ldots, M_{I_n}) = M_S\{g\beta B + \sum_i^n A_i \cdot M_{I_i}\} \tag{4.3}$$

The selection rules for the EPR transitions defines that $\Delta M_S = \pm 1$ and $\Delta M_I = 0$. From these rules the resonance condition follows, if a radiation quantum of specific energy is absorbed by the system:

$$h\nu = g\beta B + \sum_i^n A_i \cdot\ M_{I_i} \tag{4.4}$$

where M_I is the effective spin value for the corresponding number of equivalent nuclear spins. The positions of the hyperfine structure lines in the spectrum are calculated by adding or distracting a number of hyperfine constant units, which are quantized along states of the nuclear spin as follows:

$$B_i = B_0 - \sum_i^n A_i \cdot\ M_{I_i} \tag{4.5}$$

After that, characteristic absorbtion line function is fitted to the calculated line positions. Usually the Lorentz type function or it's first derivative is used:

$$y(B) = Y_{max} \frac{\Gamma^2}{\Gamma^2 + (B - B_r)^2} \tag{4.6}$$

kur Γ – halfwidth of the absorption line, Y_{max} – maximum of the absorbtion line: $Y_{max} = 1/\pi\Gamma$, B_r – magnetic field at the resonance. Usually the first derivative of this function is used:

$$y'(B) = -Y_{max} \frac{2\Gamma^2(B - B_r)}{[\Gamma^2 + (B - B_r)^2]^2} \tag{4.7}$$

The following specialized PC software have been used for the spectral simulations: EPR-NMR [34], Easyspin [35] and PCS.

Chapter 5

Results and discussion

5.1 Perturbed Cd^+ centre in the BaF_2 crystals

During the EPR experiments at room temperature we studied the samples in various orientations of the magnetic field in the X microwave band ν=9.61 Ghz ±0.01 GHz. The crystal was mounted with its [100] direction parallel to magnetic field. The orientation was changed by increment by angle of 5° rotating it counterclockwise. Hence we could obtain the angular dependency of EPR signal along all the main crystallographic directions – [100], [111], [110]. The experimental EPR spectra along the main directions are shown in figure 5.2.

In the case, if B_0 $\|$[100], eight spectral lines could be clearly seen. Their intensities have binomial distribution, however, linewidths are comparatively large ~45 MHz.

Similar situation could be observed in the EPR spectrum along the [111] direction. Eight larger line groups with hyperfine structure could be clearly resolved, and they tend to split even more towards the higher magnetic field. Anisotropy of the hyperfine splitting is partially obscured due to wide linewidhts of this spectrum. In the spectrum along the [110] direction anisotropy of the hyperfine structure could be clearly seen, however details are obscured by large linewidths.

Theoretical simulations of the EPR spectra have been done using computer programs PCS and EPRNMR. Spin Hamiltonian parameters, which were used in our calculations, are listed in the table 5.1. All effective values of the hyperfine constants for every specific direction have been calculated by (2.11).

In the figure 5.3, simulated spectra of the perturbed Cd^+ center are shown. In the perturbed center model, an unpaired electron has interaction with 7 nearest surrounding fluorine ^{19}F nuclei ($I = 1/2$). Calculated spectrum for the [100] direction consists of $k = (2nI + 1) = 8$ hyperfine lines. Positions and intensities of the lines have good coincidence with the experimental spectrum in the same direction. Line intensities follow the binomial distribution and have their corresponding weights $1 : 7 : 21 : 35 : 35 : 21 : 7 : 1$ (see figure 2.5).

Parameters of the paramagnetic center	$B \parallel [100]$	$B \parallel [111]$	$B \parallel [110]$
Magnetic field, Gs	3000 ÷ 3900		
Number of nuclei in the shell	7 ($\theta = 54.5°$)	1 ($\theta = 0°$) 6 ($\theta = 71°$) un 2 ($\theta = 0°$) 5 ($\theta = 71°$)	3 ($\theta = 90°$) 4 ($\theta = 35.5°$) un 4 ($\theta = 90°$) 3 ($\theta = 35.5°$)
g-factor	1.9896		
Electronic spin S	1/2		
Fluorine nuclear spin I^F	1/2		
^{19}F A^F_{eff}, MHz	225.6	287.9 ($\theta = 0°$) 199.3 ($\theta = 71°$)	186.0 ($\theta = 90°$) 258.9 ($\theta = 35.5°$)
Chlorine nuclear spin I^{Cl}	3/2		
^{35}Cl, ^{37}Cl A^{Cl}_{eff}, MHz	22.6	29.0 ($\theta = 0°$) 20.0 ($\theta = 71°$)	18.6 ($\theta = 90°$) 26.0 ($\theta = 35.5°$)
Bromine nuclear spin I^{Br}	3/2		
^{79}Br, ^{81}Br A^{Br}_{eff}, MHz	112.5	143.5 ($\theta = 0°$) 100.0 ($\theta = 71°$)	93.0 ($\theta = 90°$) 129.5 ($\theta = 35.5°$)
^{111}Cd nuclear spin ^{113}Cd nuclear spin	1/2 1/2		
^{111}Cd *hf* constant A, GHz ^{113}Cd *hf* constant A, GHz	10.04 [7] 10.51 [7]	–	–

Table 5.1. *EPR parameters of the Cd$^+$ center in the BaF$_2$ crystal.*

Other spectral simulations along orientations [111] and [110] also have a good coincidence with the experimental spectra. However, calculations do not reveal full details of the spectra. For example, two lines at 3420 Gs and 3610 Gs do not appear in the simulated spectra along the [110] direction.

Let us discuss briefly other hypothesis, which assumed that some other halogen ion – chlorine (^{35}Cl, ^{37}Cl) or bromine (^{79}Br, ^{81}Br) is substituting a fluorine in it's vacancy was tested. Parameters used in the calculations for this hypothesis are shown in table 5.1. Simulated spectra have a good qualitative coincidence with the experimental spectra, however, the shape of calculated spectral lines are somewhat different.

All experimental and theoretical results show that unpaired electron of the Cd$^+$ ion has a strong hyperfine interaction with 7 fluorine nuclei. As a direct evidence of number of nearest fluorine nuclei is the EPR spectrum along [100] direction, where the hyperfine structure of $k = 2nI + 1 = 8$ lines is clearly seen (see figure 5.2). Theoretical calculations within this model support our hypothesis. Discrepancies between experimental and

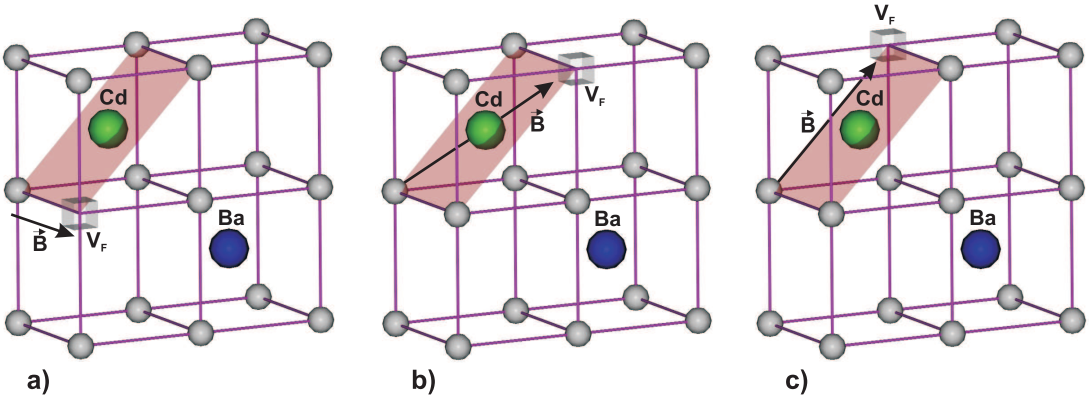

Figure 5.1. *Model of the structure of the perturbed Cd$^+$ center.*

simulated spectra, which are observable in other orientations [111] and [110] are due to perturbed nature of the hyperfine interaction of the paramagnetic center. If the fluorine vacancy is present in the nearest surrounding of cadmium, it is possible that Cd$^+$ ion has relaxed towards other fluorine atoms, due to the electrostatic interaction.

Concerning other possible impurities in the BaF$_2$ lattice – chlorine, bromine or even oxygen, question remains still open. Calculations showed that the hyperfine interaction contribution of these ligands is not sufficient to explain structure of the experimental EPR spectra. Spin of the chlorine ^{37}Cl is $I = 3/2$ which leads to additional splitting of each *hf* line into four. However, this hasn't been observed experimentally since chlorine hyperfine interaction constant is nearly two times smaller than the experimental linewidths.

A presence of the bromine, instead of fluorine, in the vacancy is even less probable. Bromine ligands has a large hyperfine interaction constant (see table 5.1). Due to this, a number of the spectral lines in the spectra should be considerably increased, since its nuclear spin is $I = 3/2$, however, no increased number of lines could be observed.

Thus, the fluorine vacancy is considered as the most probable model for the perturbed Cd$^+$ center. Vacancy should be located in the [111] direction of the BaF$_2$ crystal. The corresponding model is presented in the figure 5.1.

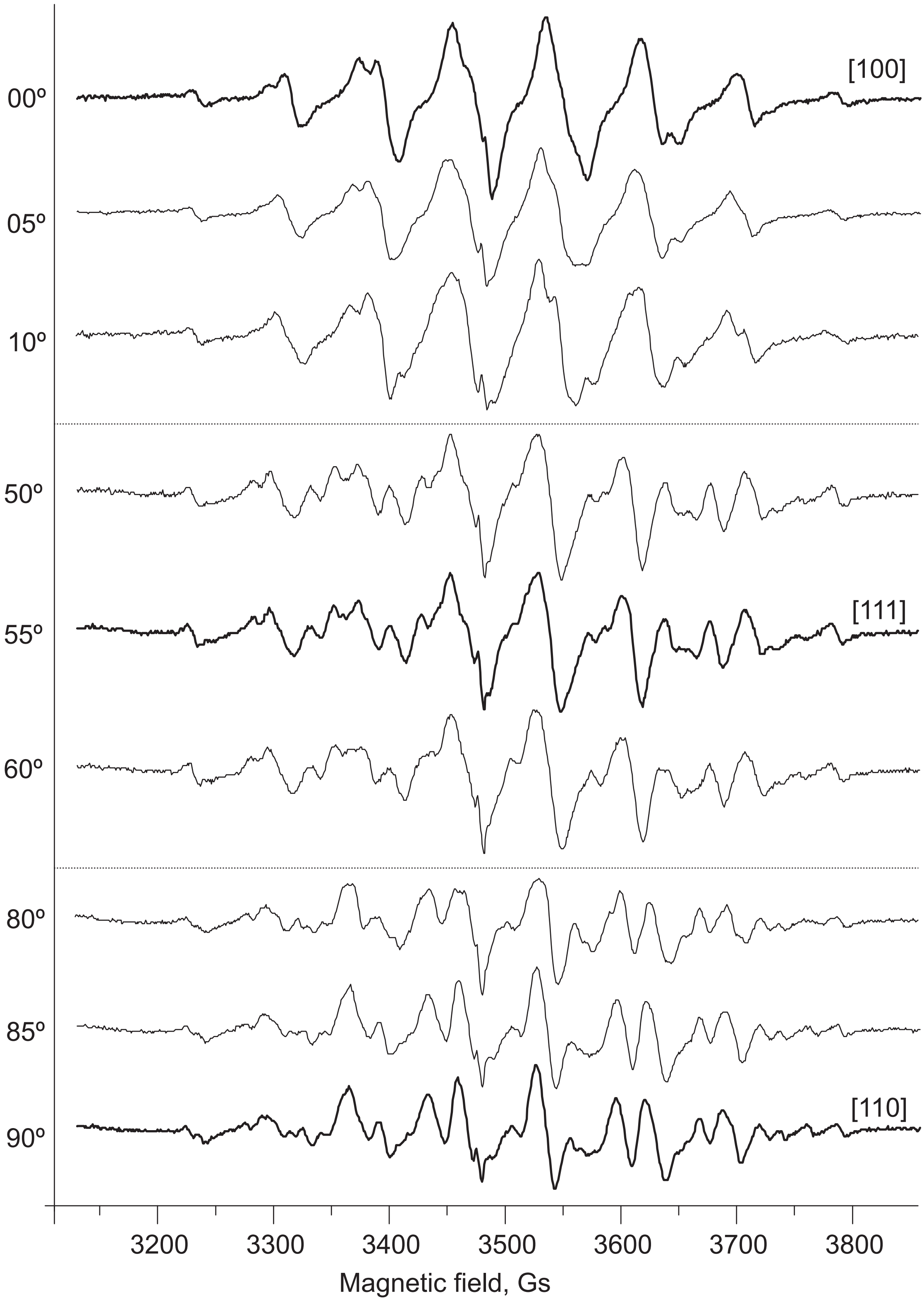

Figure 5.2. *Experimental EPR spectra of the perturbed Cd$^+$ center in the BaF$_2$ crystal.*

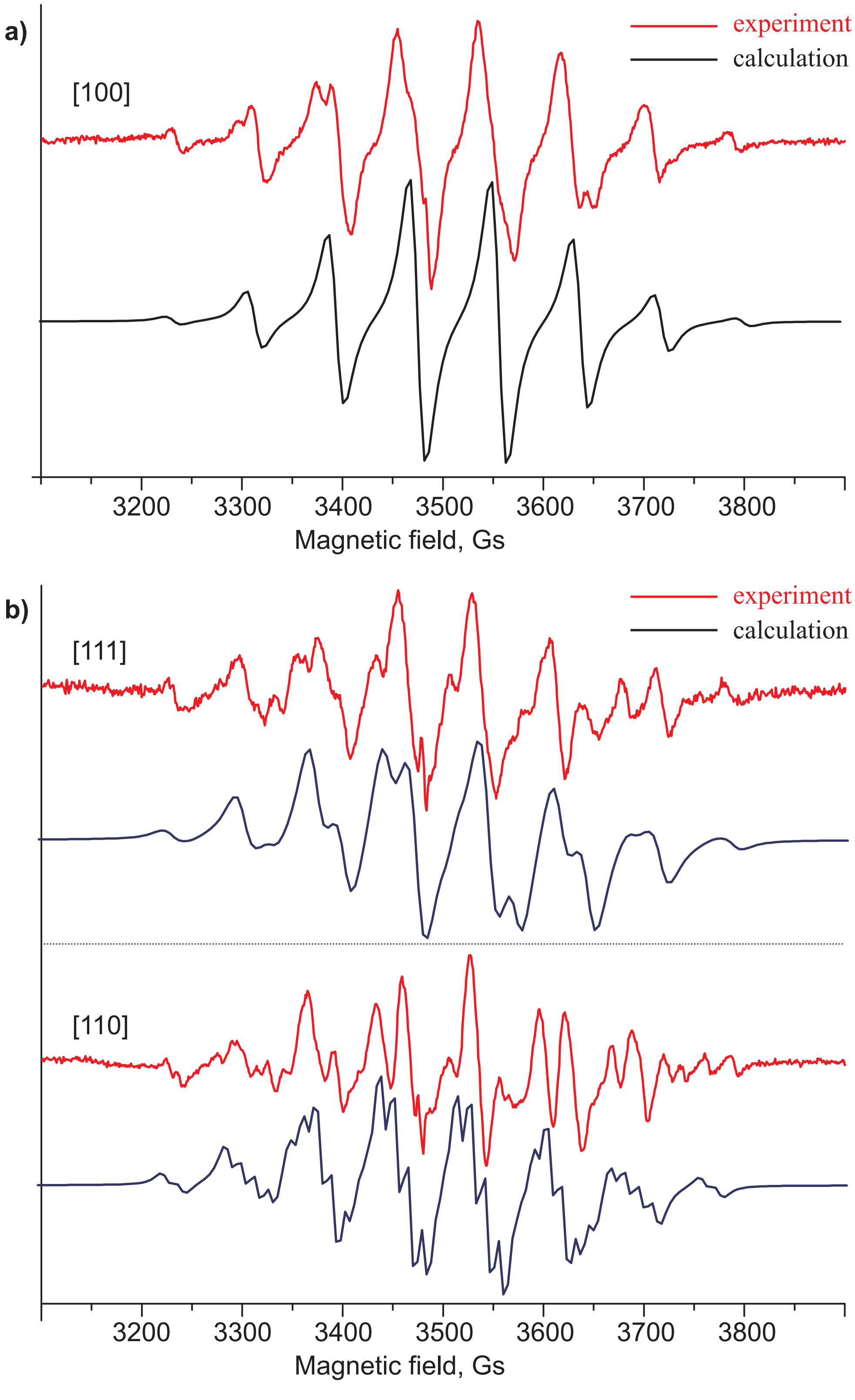

Figure 5.3. *Theoretical and experimental spectra of the perturbed Cd$^+$ center in the BaF$_2$ crystal.*

5.2 EPR of F-type centres in LiBaF$_3$ crystals

Experimental EPR spectra of our measurements are shown in the figure 5.5. All hyperfine structure lines belonging to the F-type center are well resolved contrary to the previous EPR investigations of Fe doped LiBaF$_3$ crystals [10, 36], where a broad central line, not belonging to an F-center, overlapped spectra considerably.

The EPR spectrum in the figure 5.5 is simplified at the orientation of the magnetic field B$\|$[111] and in this orientation it has nearly binomial distribution of the line intensities, similarly as in the Fe-doped crystals [10, 36]. For other orientations of the magnetic field, the line intensity decreases and spectrum broadens, the line separation remains nearly constant for all angles. The angular dependence of the EPR line intensities, showed in figure 5.5, is very strong, and the angle variations of 5° can change the spectra considerably. However, there are still close similarities with the EPR spectra of the F-type centers in the Fe-doped LiBaF$_3$ [10, 36]. Therefore, we used the same model for the F-type center as previously (see figure 5.4) and analyzed EPR spectra for the relevant orientations B$\|$[111], B$\|$[110] and B$\|$[100] with the spin Hamiltonian:

$$\hat{H} = \mu_B \mathbf{B}\hat{g}\hat{\mathbf{S}} + \sum_{i=1}^{8} \hat{\mathbf{S}}\hat{A}_i^F \hat{\mathbf{I}}^F + \sum_{j=1}^{2} \hat{\mathbf{S}}\hat{A}_j^{Li} \hat{\mathbf{I}}^{Li} \tag{5.1}$$

where $\hat{g}$, $\hat{A}_i^F$, $\hat{A}_j^{Li}$ are the g-tensor and hyperfine interaction tensors, respectively, and μ_B is the Bohr magneton. Given F-type center model explains the experimental spectra by hyperfine interaction of the electron spin $S = 1/2$ with two equivalent ^{7}Li nuclei with $I = 3/2$ (nat ab. 92.5%) and eight fluorine ^{19}F nuclei with $I = 1/2$ (nat. ab. 100%). The *hf* parameters are shown in the table 5.2. These *hf* parameters have usual meaning, i.e. $A_\perp = a - b$ and $A_\| = a + 2b$.

Figure 5.6 shows experimental spectra and simulated spectra, respectively, for the B$\|$[100], B$\|$[111] and B$\|$[110] orientations of the magnetic field. It is seen, that there is a good quantitative coincidence of the line positions and a qualitative coincidence of the line intensities, taking into account how strong are changes in the spectra by variation of the angle of 5°. In our previous reports we already suggested that the g-tensor of the F-type center could be aligned along the [100] direction of LiBaF$_3$ crystal, however the g-tensor values were not determined unambiguously, due to the overlap of the EPR spectrum with strong unidentified lines.

In the present studies, the g-tensor components take into account the g-tensor values obtained from the MCD-EPR investigations [37]. In the work [37] the angular behavior of the MCD-EPR lines of two F-type centers, one created at x-irradiation at RT, and the second one, created at 4.2 K, was very similar. Therefore, here we used the g-tensor values $g_\perp = 1.980$, $g_\| = 1.955$, obtained in [37] for low temperature center, for qualitative analysis of the EPR spectra shown in the figure 5.5, for magnetic field orientations B$\|$[100] and B$\|$[110].

Isotope	I	a, mT	b, mT	number	nat. abundancy
^{19}F	1/2	3.58 3.12 [36]	0 0.20 [36]	8	100%
^{7}Li	3/2	0.89 0.91 [36]	0 0.03 [36]	2	92.5%

Table 5.2. *Spin Hamiltonian parameters of the F-type center in the LiBaF$_3$ crystal.* hf *constants are given in mT. Comparison with results from previous works have been given.*

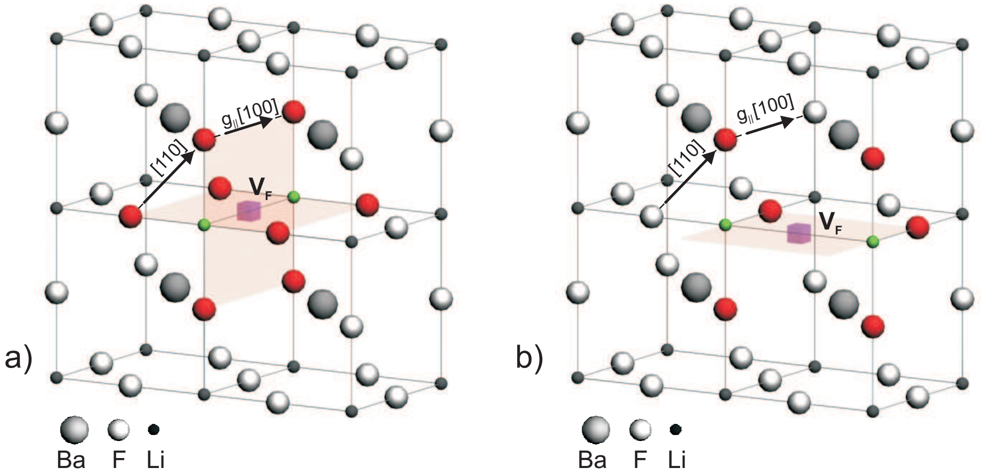

Figure 5.4. *F-type center model in the LiBaF$_3$ crystal.*

We reconsidered also the anisotropy of the hyperfine interactions, earlier [10, 36] it was taken to be the same as for the F-center in LiF [38]. In the present investigation, we found out, that the anisotropic part of the *hf* interactions should be reduced to nearly zero values, because otherwise it was not possible to avoid additional line splitting in the spectra [1]*. With these isotropic *hf* values, listed in the table 5.2, we found a good coincidence between the experimental and calculated spectra, especially taking into account, that at the orientation B||[100], the line group with g_{90} has a “double weigh”, compared to the line group with the g-value g_0. Thus, the angular dependence of the spectra has been explained by an anisotropic g-tensor and nearly isotropic hyperfine interactions. These results gives further support to the F-type model for the radiation defect created in the LiBaF$_3$ by the X-irradiation at RT. This F-type center has two Li and eight fluorine neighbors in the first two shells, however a perturbation in the third or further neighbor shells could not be excluded by the EPR.

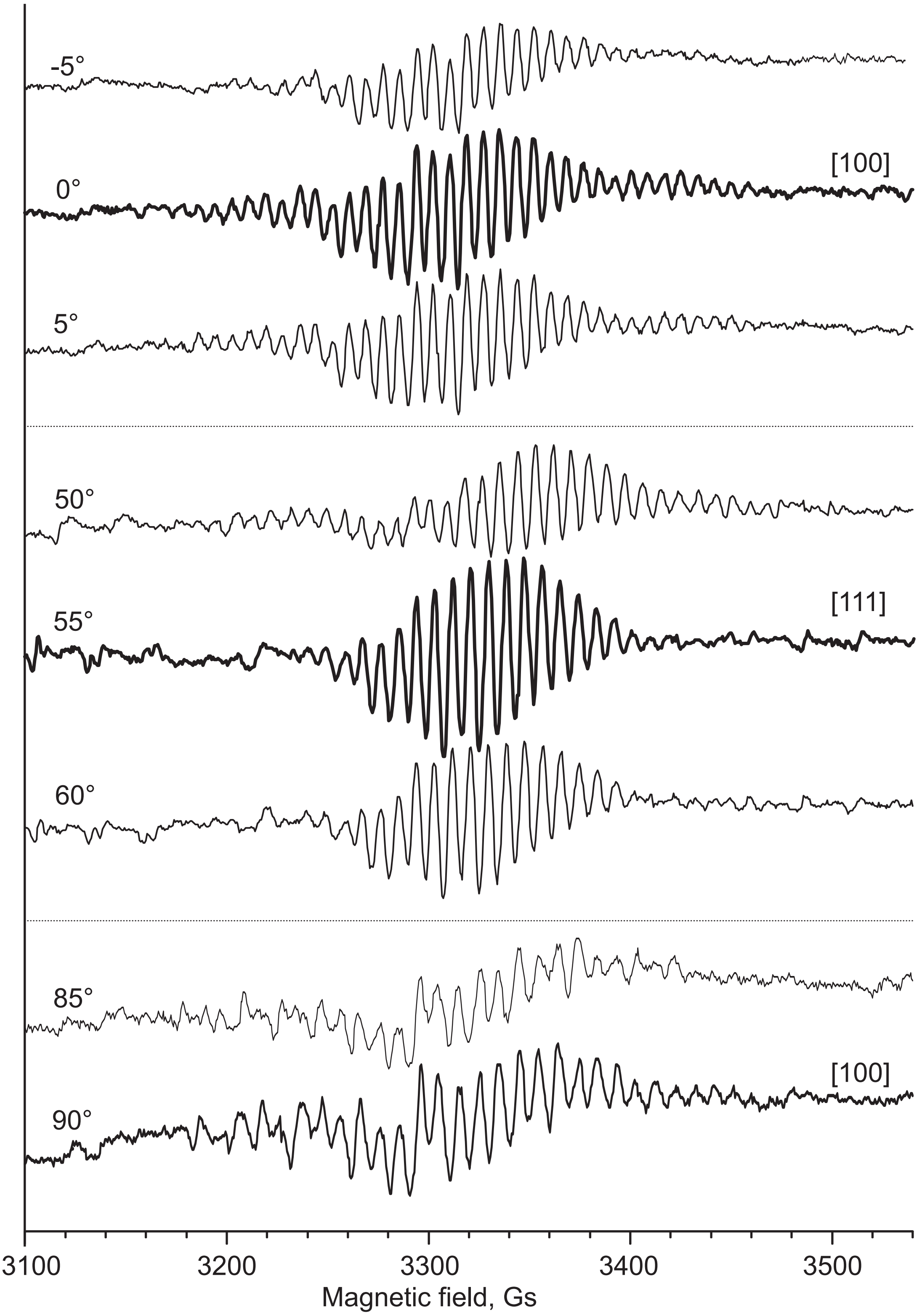

Figure 5.5. *Experimental spectra of the X-irradiated* $LiBaF_3$ *crystal along the main crystallographic directions.*

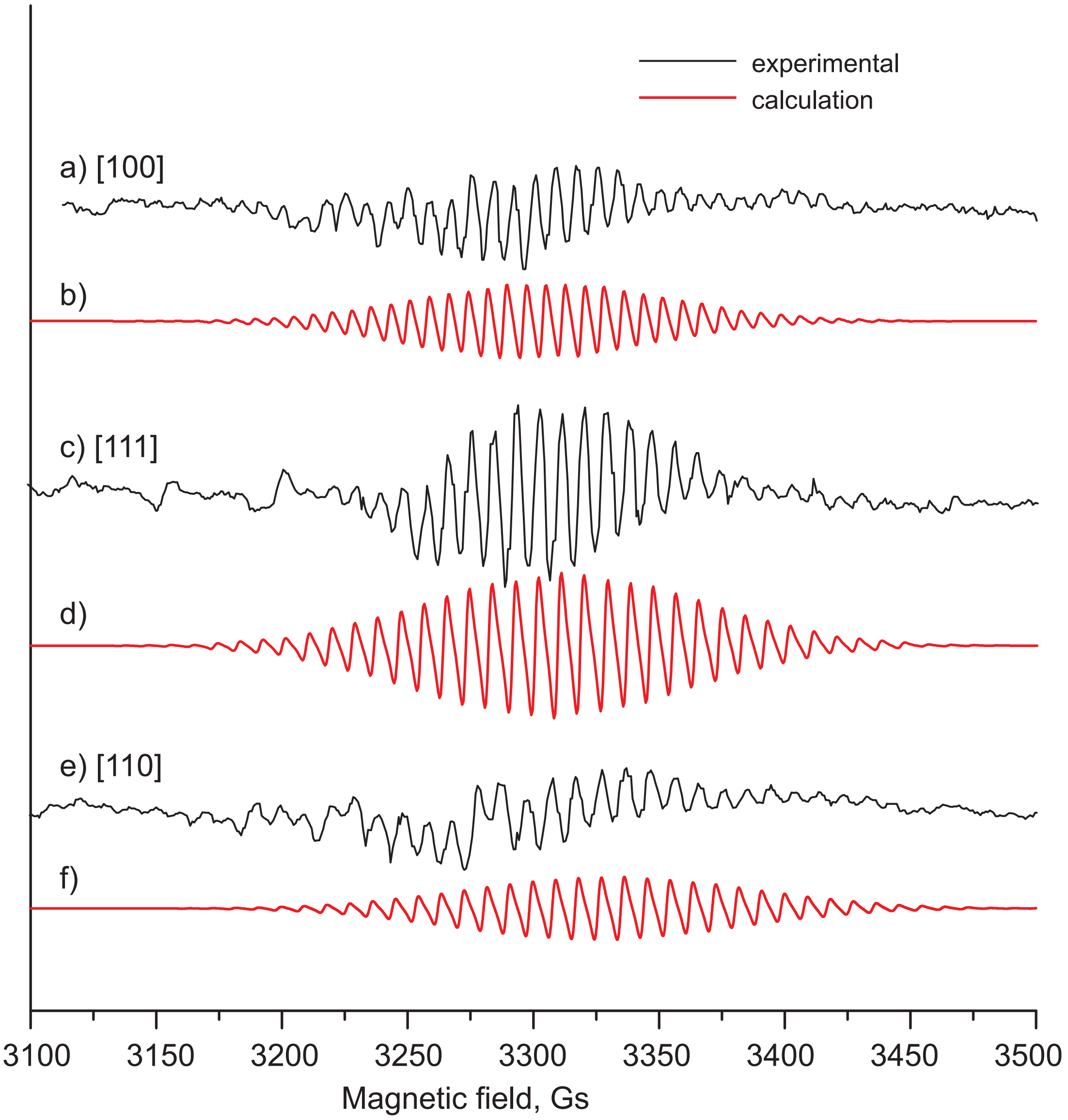

Figure 5.6. *Experimental and theoretically simulated EPR spectra of the F-center in the LiBaF$_3$ crystal.*

5.3 EPR of radiation defects in LiYF$_4$ crystals

No EPR signals could be detected in the non-irradiated sample at RT measurements. Nevertheless, an intensive line near 3500 Gs – indicating the presence of residual impurity, with a strong g-factor anisotropy, has been observed at 77 K. After irradiation at RT, an additional broad line appeared in the RT measured spectra at 3370 Gs with $g \sim 2$. Low-temperature measurements of the RT irradiated sample have resolved a more detailed structure of the EPR spectra of the radiation-induced center. Detailed investigation into the angular dependence of this center's spectrum showed, that it consists of two to four lines at about 3250-3310 Gs at 9.15 GHz, depending on the orientation of the magnetic field (see figure 5.7). In figure 5.7 three EPR lines are observed in the orientation $\mathbf{B} \parallel c$. Only two intense lines are observed in the orientation $\mathbf{B} \perp c$. Splitting of EPR lines varies as sample is rotated from these orientations by increment of 5°. Similar situation has been observed in the second measurement series, if the magnetic field B was rotated in the plane ab. The spectral line of the impurity center at this orientation does not exhibit angular dependence and is located at 3495 Gs. The line width remains almost the same during measurements and is approximately 6 Gs (see figure 5.8). Further investigation has shown that the color center is stable at room temperature and does not decay even after its long exposure to daylight. Irradiation and measurements of the crystal at 77 K did not lead to the appearance of additional lines in the EPR spectra, as it occurred in the previously observed V$_K$ center spectrum [19].

To analyze the spectra of a radiation defect and their angular dependencies, we used the following spin Hamiltonian:

$$\hat{\mathscr{H}} = \mu_B \cdot \mathbf{B} \cdot \hat{g} \cdot \mathbf{S} + \sum_{i=1}^{2} \mathbf{S} \cdot \hat{A} \cdot \mathbf{I}_i \tag{5.2}$$

where μ_B is the Bohr magneton, $\hat{g}$ is an axial g-tensor, A describes a hyperfine interaction between the unpaired electron spin $S = 1/2$ and two fluorine nuclei ^{19}F ($I = 1/2$, nat. abundance 100%). For a simplicity, in the present investigation we assumed A to be isotropic and equivalent for the interaction with both fluorine nuclei.

For the magnetic field orientation $\mathbf{B} \parallel c$, the calculated spectrum is shown in the figure 5.8 (curve b), assuming $A = 10.0$ Gs. The following g-tensor component values have been used: $g_\perp$=2.00 and $g_\parallel$=1.975. From the angular dependencies we have estimated the angle between the g-tensor's main axis z and the fourfold axis c of the crystal to be about $\varphi = 65°$.

The main features peculiar to the EPR spectra of the defect created by X-irradiation at RT are: it has a partially resolved irregular structure at 77 K, consists of at least four sub-lines, and is anisotropic in two rotation planes. As mentioned, the defect is stable at RT.

According to the estimated g values, which are close to $g = 2.0$, the EPR spectrum of the observed radiation defect could belong to an electron trap centre. The F-center (a

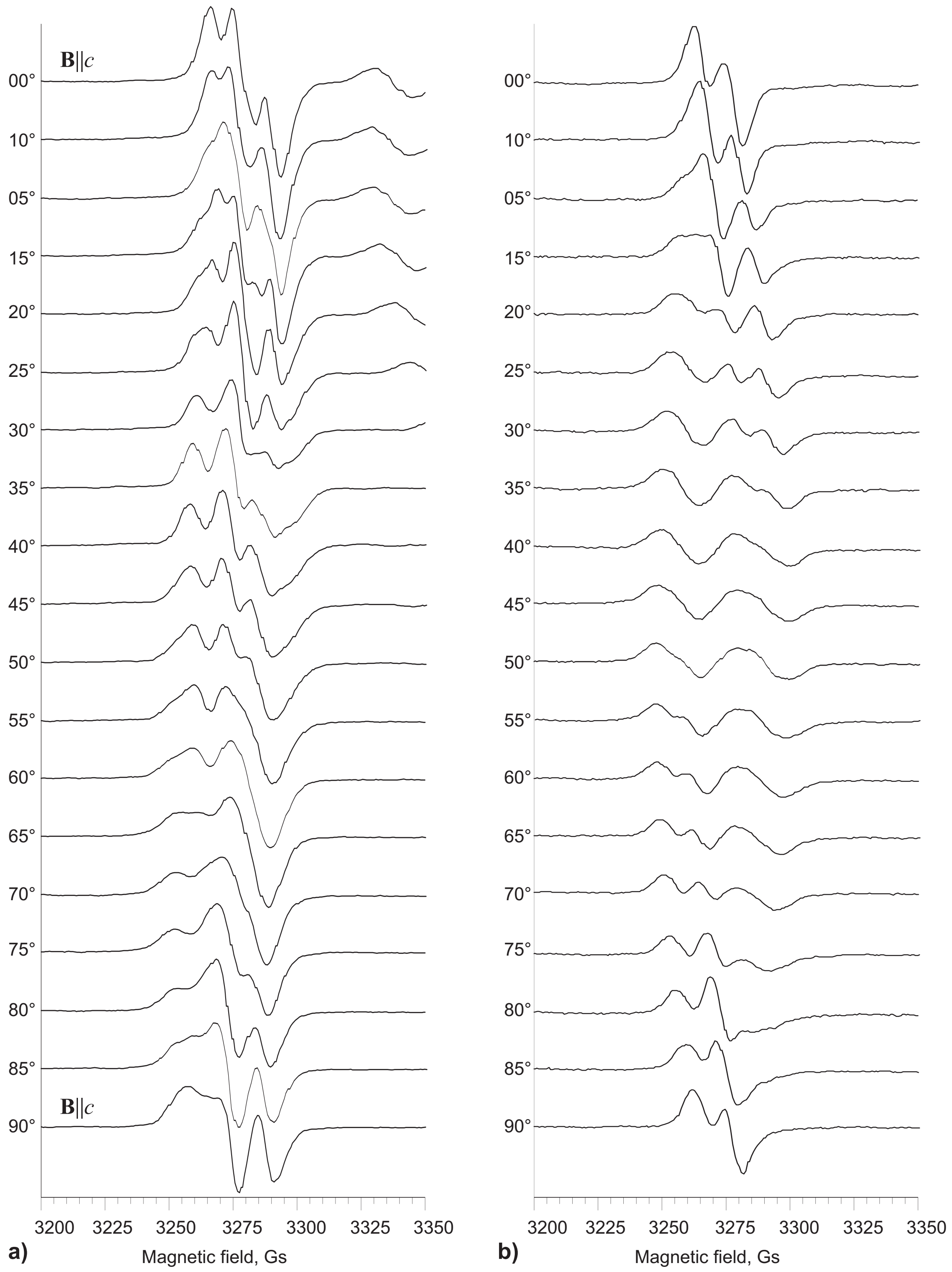

Figure 5.7. *Experimental spectra of radiation defect in the LiYF$_4$ crystal, for magnetic field directions: a)from $\mathbf{B} \parallel c$ to $\mathbf{B} \perp c$, b)in the plane* ab*, rotating crystal around* c *axis.*

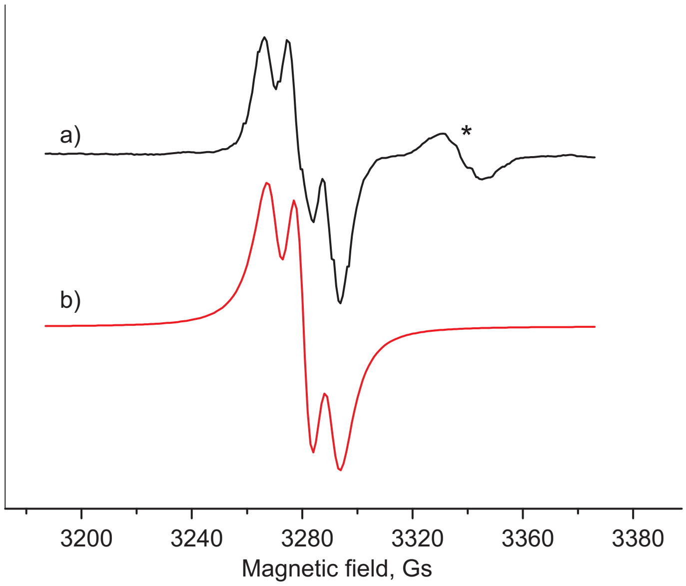

Figure 5.8. *Experimental a) and calculated b) EPR spectra for the orientation* $\mathbf{B} \parallel c$.

fluorine vacancy with a trapped electron) would be considered as a most possible model for this defect.

Examination of the LiYF$_4$ structure (see figure 3.4) shows that the fluorine vacancy has at least four neighboring fluorine ligands at four different distances [18]. The fluorine hyperfine interaction is expected to be the main source of *hf* structures in LiYF$_4$, like in other fluorides. Since *hf* interaction is strongly dependent on the inter-nuclear distance in LiYF$_4$, it should not exhibit such regular *hf* behavior between paramagnetic centers as it is in the case of LiBaF$_3$ and LiF [36,38], [1]*. It is possible that *hf* interaction from some of the fluorine neighbors dominate. The observed anisotropy of the spectra could rather been explained by a g-tensor anisotropy and nearly isotropic hyperfine interaction with two fluorine nuclei. The main axis of the g-tensor in the LiBaF$_3$ is in the Li direction [36], [1]*; this is possible also in the case of LiYF$_4$: one Li ion is the nearest to the arbitrary fluorine ion. F-Li directions in the structure of LiYF$_4$ do not coincide with the symmetry axis c, but deviate from it; due to the crystal symmetry, there should be four magnetically nonequivalent directions of F-centers, with respective g-tensors. The number of lines in the observed spectra indicates the presence of such four differently oriented centers.

Indeed, the analysis of the structure and angular dependencies of the EPR spectra of the radiation defect gives a reasonable set of parameters: $g_{\parallel} = 2.00$, $g_{\perp} = 1.975$, $A = 10$ Gs, where the main axis of g-tensor is aligned at the angle $\varphi = 65^{\circ}$ in respect to the fourfold symmetry axis c of the LiYF$_4$. Calculations with this set of parameters give a qualitative reproduction of the experimental spectra (see figure 5.8). However, a further improvement of the parameter set should be done, particularly taking into account the possibility that A constant may be slightly anisotropic.

5.4 EPR of radiation defects in OxFGC

EPR spectra of radiation induced defects have been obtained in both glass and glass-ceramics materials. No EPR signal could be detected prior to the irradiation. After the irradiation, various absorption lines appeared in the EPR spectra (see figure 5.9). Comparing the EPR spectra of the glass and the glass-ceramics, considerable qualitative additional features could be observed in the glass-ceramics: 1) an intense line at 1500 Gs, which could probably be attributed to a Fe^{3+} impurity, common in oxide glasses, 2) two broad bands between 1500 Gs and 3000 Gs, 3) two broad lines at 3250 Gs, one with a g-factor $g = 1.975$, obscuring partially resolved hyperfine structure of the spectrum (see details in the figure 5.10). A sharp line at 3200 Gs is common in both material states and is attributed to some typical irradiation defect in silicate glasses. Radiation induced defects in oxyfluoride glass ceramics, in which crystallites have not been yet created, show no explicit *hf* interaction of fluorine nuclei. Hyperfine lines could be resolved only at 77 K and after warming to RT, the *hf* structure in the spectrum disappears.

To separate the EPR spectra of the glass and the glass-ceramics spectra, the glass spectrum was subtracted from the spectra of the glass ceramics (see curve c in figure 5.9) so a distinction between both is seen in more details.

There are several possibilities for creation of crystalline phases. Most probable phases are as following: oxides — $LiYSiO_4$, Y_2SiO_5, Li_2SiO_3 and fluorides -- YF_3, LiF and $LiYF_4$. It is well known, that *hf* interaction with fluorine nuclei often leads to a well-pronounced *hf* structure in the EPR spectra. EPR of intrinsic defects induced with irradiation in fluoride single crystals are well studied [36–38], [1, 2]*. g-factor <2 indicates that our discussed defect is rather an electron center. In our case, an F-type center as a most probable model could be considered. Similar centers have been reported in LiF and $LiBaF_3$ [36–38], [1]*.

The following spin Hamiltonians could describe the interaction of a paramagnetic electron with its nearest surrounding ions with nonzero nuclear spins, in the case of the interaction with fluorine and lithium ions:

$$\hat{\mathscr{H}} = \mu S\hat{g}B + \sum_{i=1}^{N_F} SA_i^F I_i^F + \sum_{j=1}^{N_{Li}} SA_j^{Li} I_j^{Li} \tag{5.3}$$

$$\hat{\mathscr{H}} = \mu S\hat{g}B + \sum_{i=1}^{N_F} SA_i^F I_i^F + \sum_{j=1}^{N_Y} SA_j^Y I_j^Y \tag{5.4}$$

Nuclear spins of possible fluoride crystalline components are $I^Y = 1/2$, $I^F = 1/2$, $I^{Li} = 3/2$ (only ^{7}Li isotope is taken into account). A number of specific nuclei is denoted with N_F, N_Y and N_{Li}, respectively. For evaluation of a proper number of nearest neighbors, a crystalline structure of possible crystalline phases should be considered. Hyperfine structure in this case should be caused by a certain number of equidistant fluorine

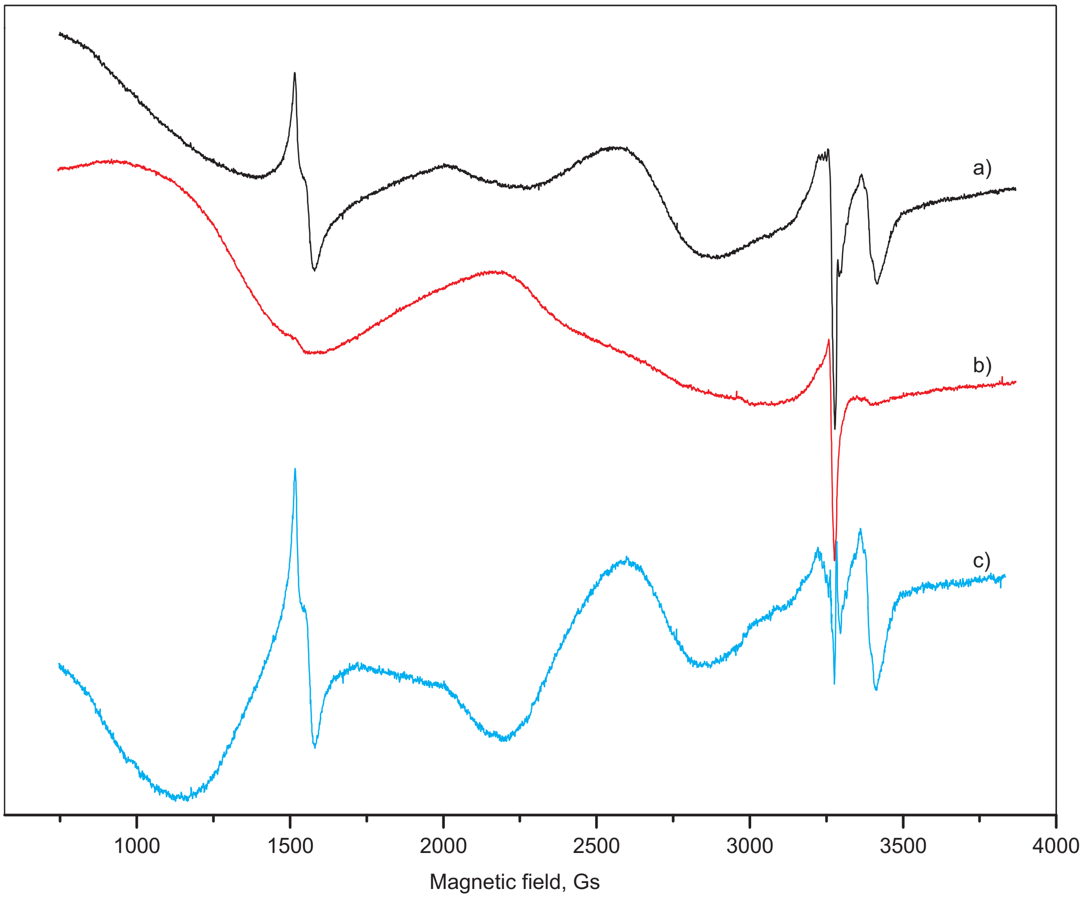

Figure 5.9. *Experimental X-band EPR spectra of radiation defect in: a) oxyfluoride glass-ceramics (GC), b) oxyfluoride glass (G) and c) in crystalline phase of glass-ceramics (C), measured at 77 K after X-irradiation at RT.*

Isotope	Nat. abund. %	nuclear spin I	A, MHz	number
^{19}F	100	1/2	56.02	10
^{89}Y	100	1/2	23.025	4
^{7}Li	92.58	3/2	-	-

Table 5.3. *Spin Hamiltonian parameters which could describe a F-type center in the YF_3 crystal.*

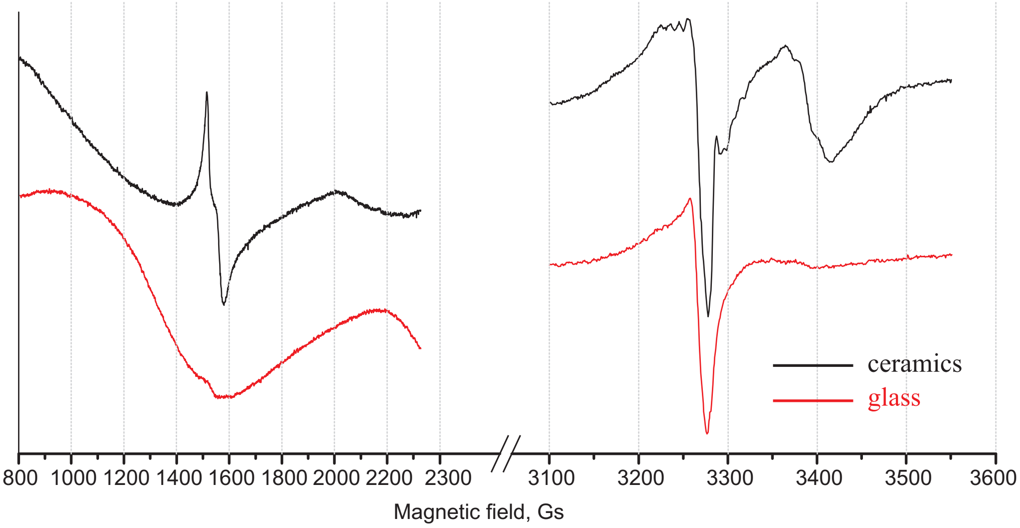

Figure 5.10. *EPR spectra of radiation defects, shown in more details.*

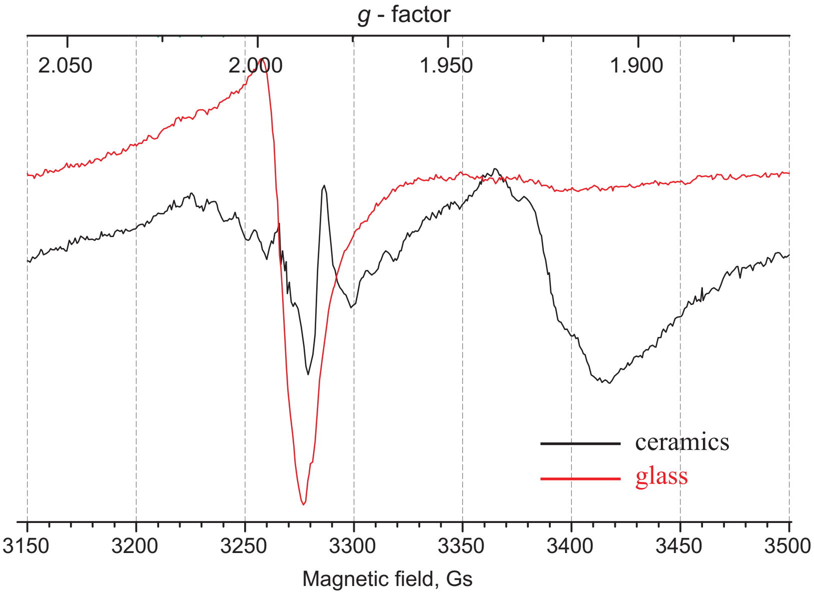

Figure 5.11. *A part of the experimental EPR spectra of radiation defects in oxyfluoride glass (G) and glass-ceramics, whereby only the crystalline part (C) is shown.*

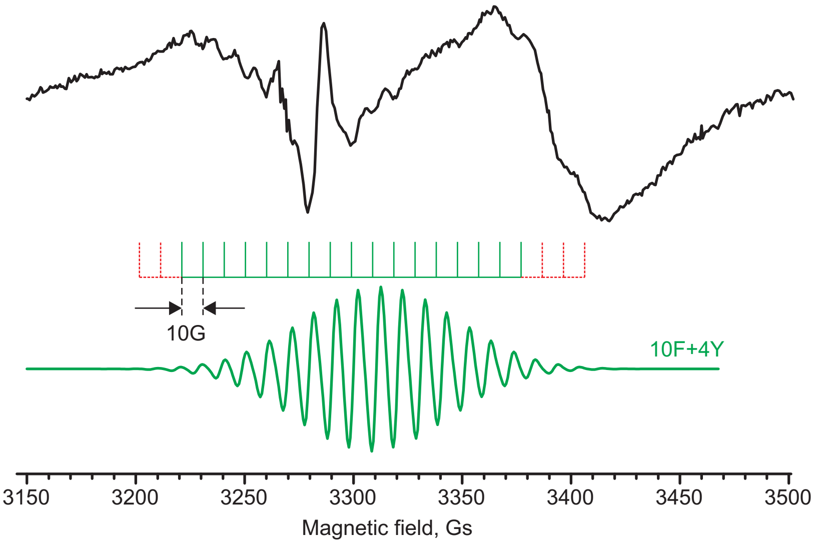

Figure 5.12. *Experimental EPR spectra of radiation defect in oxyfluoride glass and glass-ceramics, compared with a simulated EPR spectrum, taking into account an hf interaction with 10 fluorine and 4 yttrium nuclei.*

nuclei N_F, equidistant yttrium nuclei N_Y and/or equidistant lithium nuclei N_{Li}. Since the *hf* structure of the spectrum is partially obscured by the two broad EPR lines, we cannot precisely resolve the number of lines. Thus we base our simulated spectra on a qualitative coincidence with the common width of the spectrum and relative intensities of the *hf* structure lines. The most probable model of the crystalline phase would be that of YF_3. It allows us to consider a *hf* interaction of the electron with $N_F = 10$ and $N_Y = 4$ nuclei. In the table characteristic spin Hamiltonian parameters for F-type center are shown. Resulting simulated spectrum shows a rather good coincidence with the experimental spectrum (see figure 5.12). Other possibilities, which included an *hf* interaction with Li nuclei, do not seem so reasonable. In any case, by adding of two lithium nuclei to the model, the number of fluorine nuclei should be decreased by at least three nuclei, which is not reasonable in any considerable model of the crystalline phase.

The *hf* structure of the F-centre in LiF includes a *hf* interaction with six ^{7}Li and two ^{19}F nuclei [38], but the F-type center in $LiBaF_3$ possess the *hf* interaction with two ^{7}Li and eight ^{19}F nuclei [1]*. Thus, the Li *hf* interaction has been excluded from our present analysis. The XRD data on our samples confirm possibility of both YF_3 and $LiYF_4$ phases in the material. However, it is still not clear, which crystallographic structure obtained crystallites could possess.

Chapter 6

Conclusions and theses

6.1 Main results

1) An hyperfine interaction and its angular dependence of the perturbed Cd^{+} impurity center have been investigated in the BaF_2:Cd^{+} crystal.

2) A nature of the hyperfine interaction and the g-factor anisotropy of the F-type center have been investigated and concretized for the $LiBaF_3$ crystal of high purity.

3) The hyperfine interaction and the g-factor anisotropy have been investigated and clarified in the pure $LiYF_4$ crystal.

4) An EPR spectrum, characteristic to the ^{19}F nuclei hyperfine interaction, have been observed and investigated in details in the oxyfluoride glass-ceramics.

6.2 Conclusions

1) In the irregular Cd^{+} impurity center in a BaF_2 crystal, the hyperfine interaction with one of the neighboring ^{19}F nuclear spins is missing.

2) The spectra of the X-ray induced F-type center in the high purity undoped $LiBaF_3$ crystal have been observed in details. Theoretical calculations confirms the hypothesis about the g-factor anisotropy of the center with the following g-values: $g_{\parallel} = 1.955$ and $g_{\perp} = 1.98$.

3) EPR spectra of the radiation defect in the $LiYF_4$ crystal could be explained within a model of the F-type center, where localized unpaired electron has an *hf* interaction with two nearest ^{19}F nuclei, and axial g-tensor with following components: $g_{\parallel} = 2.00$ un $g_{\perp} = 1.975$.

4) The hyperfine structure of the EPR spectrum in the OxFGC could be explained within a model of an intrinsic radiation defect – F-type center in the YF_3 crystalline phase. Following isotropic EPR parameters have been estimated: $g = 1.975$, $A^F = 56$ MHz, $A^Y = 23$ MHz.

6.3 Main theses

1) A perturbed nature of the EPR spectra in the γ-irradiated BaF_2:Cd^+ crystal is caused by one fluorine deficiency in the nearest surrounding of the Cd^+.

2) Observed angular dependance of the electron trap center in the X-irradiated $LiYF_4$ crystal could be explained by the anisotropy of the g-factor and dominating *hf* interaction with two nearest fluorine nuclei.

3) The hyperfine structure of the EPR spectrum of the radiation defect in the OxFGC could be explained within a model of an intrinsic radiation defect – F-type center in the YF_3.

6.4 Outlook

Investigations of the present work have let to explain structure of specific defects in the fluoride crystal matrixes. Paramagnetic centers in the fluoride crystals are formed due to an electron localizing in the anion vacancy (F-type centers) or on some definite impurity defect. In the case of fluorides, stable radiation defects are one-electron centers with $S = 1/2$, thus there is no fine structure interaction observed due to additional electron spin splitting in the crystal field. The structure of the paramagnetic centers in the fluorides is revealed by the strong hyperfine interaction with the nearest fluorine nuclei ^{19}F with $I = 1/2$. In this case, a number of nearest ligands and interaction energy could be estimated from the number of the *hf* structure lines and their intensity distributions in the EPR spectra.

In case of the BaF_2:Cd^+ crystal, the electron is localized on the Cd^+ impurity ion, which have replaced barium in the host lattice. Observed *hf* structure of the EPR spectra is perturbed, because of missing of the *hf* interaction with one of the eight nearest fluorine nucleus. Our calculations confirmed a proposed hypothesis regarding the fluorine vacancy. Other reasonable possibilities are that chlorine or bromine have replaced the fluorine. However, in such case considerable changes in the EPR spectra should be observed due to the EPR parameters of these ligands. It is still possible that the oxygen has not completely evaporated from the crystal, but this could not be confirmed by means of the EPR.

F-type centers have formed in the $\mathrm{LiBaF_3}$ and $\mathrm{LiYF_4}$ crystals after the X-irradiation at room temperature. Structure of the defect nearest surrounding could be determined from the observed *hf* structure in the EPR spectra. In case of the $\mathrm{LiBaF_3}$ there are eight ^{19}F nuclei with $I^F = 1/2$ and two ^{7}Li nuclei with $I^{Li} = 3/2$. But in case of the $\mathrm{LiYF_4}$, unpaired electron of the F-center has strong *hf* interaction with two nearest fluorine nuclei and explicit g-factor anisotropy.

One of the interesting results in our recent studies is the observed radiation center in the oxyfluoride glass-ceramics. Up to now, only studies of rare-earth impurities have been reported, and there were no available information about intrinsic defects in the crystalline compounds of these materials. We observed a creation of radiation defects in both – silicate glass matrix (host material) and in the created crystalline phases. The investigated EPR *hf* spectrum in the OxFGC could be described within a F-type center model in the $\mathrm{YF_3}$ crystalline phase. In this case, the g-factor and hyperfine constants of the center have isotropic values. However, more elaborate studies of this defect using optical spectroscopy and x-ray diffraction analysis, should be done in order to clarify the nature of the all radiation effects in these materials.

Literature

[1] Carel W. E. van Eijk, *Inorganic-scintillator development*, Nuclear Instruments and Methods in Physics Research A, **460**, (2001), pp. 1.

[2] A. Kerek, W. Klamra, L. O. Norlin, D. Novak, S. Westman, KTH, J. Lidberg, S. Mannervik, *Fast inorganic scintillators for beam diagnostics at extreme high vacuum*, Nuclear Science Symposium Conference Record, 2001 IEEE, **1**, (2001), pp. 346.

[3] M. Globus, B. Grinyov, Jong Kying Kim, *Inorganic Scintillators for Modern and Traditional Applications*, National Academy of Sciences of Ukraine (2005).

[4] Дж. Верц, Дж. Болтон, Теория и практические приложение метода ЭПР, МИР (1975).

[5] Frederick Seitz, *Color centers in alkali halide crystals. II*, Reviews of Modern Physics, **26**, (1954), p. 7.

[6] В. Ф. Крутиков, Н. И. Силкин, В. Г. Степанов, ЭПР примесных центров Cd^+ в кристаллах гомологического ряда флуорита, Физика Твердого Тела, **18**, (1976), p. 2958.

[7] U. Rogulis, J. Trokss, A. Veispals, I. Tale, P. Kulis, M. Springis, *ODMR of Cd impurity centers in γ irradiated BaF_2 crystals*, Radiation Effects and Defects in Solids, **135**, (1995), pp. 361.

[8] M. Springis, A. Veispals, P. Kulis, U. Rogulis, I. Tale, J. Trokss, *Optical and spectral properties of the Cd containing BaF_2*, Proc. Int. Conf. on Inorganic Scintillators and Their applications, Scint95, (1996), p. 403.

[9] E. Radzhabov, M. Kirm, *Triplet luminiscence of cadmium centres in alkaline-earth fluoride crystals*, Journal of Physics: Condensed Matter, **17**, (2005), pp. 5821.

[10] U. Rogulis, V. Ogorodnik, I. Tale, A. Veispals, *EPR of radiation defects in $LiBaF_3$ crystals*, Radiation Effects and Defects in Solids, **157**, (2002), pp. 699.

[11] A. Bensalah, K. Shimamura, V. Sudesh, H. Sato, K. Ito, T. Fukuda, *Growth of Tm, Ho-codoped* $YLiF_4$ *and* $LuLiF_4$ *single crystals for eye-safe lasers*, Journal of Crystal Growth, **223**, (2001), pp. 539.

[12] C. M. Combes, P. Dorenbos, C. W. E. van Eijk, C. Pedrini, H. W. Den Hartog, J. Y. Gesland, P. A. Rodnyi, *Optical and scintillation properties of* Ce^{3+} *doped* $LiYF_4$ *and* $LiLuF_4$ *crystals*, Journal of Luminescence, **71**, (1997), pp. 65.

[13] J. P. Sattler, J. Nemarich, *Electron paramagnetic resonance spectra of* Nd^{3+}, Dy^{3+}, Er^{3+} *and* Yb^{3+} *in lithium yttrium fluoride*, Physical Review B, **4**, (1971), p. 1.

[14] Vishwamittar, S. P. Puri, *Interpretation of the crystal-field parametres in rare-earth substituted* $LiYF_4$ *crystal*, Journal of Physics C: Solid State Physics, **7**, (1974), p. 1337.

[15] T. Yosida, M. Yamaga, D. Lee, T. P. J. Han, H. G. Gallagher, B. Henderson, *The electron spin resonance and optical spectra of* Ce^{3+} *in* $LiYF_4$, Journal of Physics: Condensed Matter, **9**, (1997), pp. 3733.

[16] A. Bensalah, M. Nikl, A. Vedda, K. Shimamura, T. Satonaga, H. Sato, T. Fukuda, G. Boulon, *X-ray induced color centres in pure and doped* $LiYF_4$ *and* $LiLuF_4$ *single crystals*, Radiation effects and defects in Solids, **157**, (2002), pp. 563.

[17] G. M. Renfro, L. E. Halliburton, W. A. Sibley, R. F. Belt, *Radiation effects in* $LiYF_4$, Journal of Physics C: Solid State Pysics, **13**, (1980), pp. 1941.

[18] W. Hayes, M. Yamaga, D. J. Robbins, B. Cockayne, *Optical detection of exciton EPR in* $LiYF_4$, Journal of Physics C: Solid State Physics, **13**, (1980), pp. L1001.

[19] M. Herget, A. Hofstaetter, A. Scharmann, *EPR of the* F_2^- *centre in* $LiYF_4$, Phys. Stat. Sol. (b), **127**, (1985), p. K83.

[20] М. В. Никанович, А. П. Шкадаревич, Ю. С. Типенко, Д. С. Умрейко, Исследование радиационных дефектов в кристаллах LiYF_4, Журнал прикладной спектроскопии, **58**, (1993), p. 187.

[21] М. В. Никанович, А. П. Шкадаревич, Ю. С. Типенко, С. В. Никитин, Н. И. Силкин, Д. С. Умрейко, Радиационные центры окраски в кристалле LiLuF_4, Физика Твердого Тела, **30**, (1988), p. 1861.

[22] K. J. Guedes, K. Krambrock, J. Y. Gesland, *Identification of trivalent rare earth impurities in* YF_3, LuF_3 *and* $LiYF_4$ *by electron paramagnetic resonance*, Journal of Alloys and Compounds, **344**, (2002), pp. 251.

[23] L. Dimitročenko, *Synthesis of complex fluoride single crystals, glass ceramics containing nano-crystals and their optical properties*, Ph.D Thesis, University of Latvia (2007).

[24] Yu Hua, Zhao Li-Juan, Meng Jie, Liang Qin, Yu Xuan-Yi, Tang Bai-Quan, Xu Jing-Jun, *Nanocrystal formation and structure in oxyfluoride glass ceramics*, Chinese Physics, **14**(9), (2005), p. 1799.

[25] Zhang Li-Yan, Xu Shi-Qing, Hu Li-Li, *Intense green upconversion luminscence in Er^{3+}:Yb^{3+} codoped fluorophosphate glass ceramic containing $SrTe_5O_{11}$ nanocrystals*, Chinese Physics Letters, **24**(10), (2007), p. 2945.

[26] Zhihua Li, Longzhen Zheng, Luning Zhang, Leyan Xiong, *Synthesis, characterization and upconversion emission properties of the nanocrystals of Yb^{3+}/Er^{3+}-codoped YF_3–YOF–Y_2O_3 system*, Journal of Luminscence, **126**, (2007), pp. 481.

[27] Daqin Chen, Yuansheng Wang, Yunlong Yu, En Ma, Zhongjian Hu, *Spectroscopic properties of Er^{3+} ions in transparent oxyfluoride glass ceramics containing CaF_2 nano-crystals*, Journal of Physics: Condensed Matter, **17**, (2005), pp. 6545.

[28] V. D. Rodriguez, V. K. Tikhomirov, J. Mendez-Ramos, A. B. Seddon, *The shape of the 1.55 μm emission band of the Er^{3+} -dopant in oxyfluoride nanoscaled glass-ceramics*, Europhysics Letters, **69**, (2005), pp. 128.

[29] A. Sarakovskis, L. Dimitrocenko, A. Misnevs, U. Rogulis, M. Springis, *Up-conversion process in erbium doped lithium fluoride bulk crystal, lithium borate glass and glass ceramics*, Journal of Physics: Conference series, **93**, (2007), p. 012041.

[30] Zhang Jun-Jie, Kawamoto Yoji, Dai Shi-Xun, *Infrared-to-green upconversion luminscence and mechanism of Ho^{3+}, Nd^{3+} and Yb^{3+} ions in oxyfluoride glass ceramics*, Chinese Physics, **13**(7), (2004), p. 1156.

[31] S. Gonzalez-Perez, F. Lahoz, J. M. Caceres, V. Lavin, I. da Silva, J. Gonzalez-Platas, I. R. Martin, *Energy transfer in Pr^{3+}–Yb^{3+} codoped oxyfluoride glass ceramics*, Optical materials, **29**, (2007), pp. 1231.

[32] A. Sen, S. L. Chaplot, R. Mittal, *Vibrational and thermodynamic properties of high-pressure phases in $LiYF_4$*, ArXiv Condensed Matter e-prints, cond-mat/0406427.

[33] K. Rotereau, Ph. Daniel, A. Desert, J. Y. Gesland, *The high-temperature phase transition in samarium fluoride, SmF_3: structural and vibrational investigation*, Journal of Physics: Condensed Matter, **10**, (1998), pp. 1431.

[34] Michael J. Mombourquette, John A. Weil, *Operating instructions for computer program EPR-NMR*, University of Saskatchewan, Canada (2004).

[35] Stefan Stoll, Arthur Schweiger, *EasySpin, a comprehensive software package for spectral simulation and analysis in EPR*, Journal of Magnetic Resonance, **177**, (2005), pp. 390.

[36] V. Ogorodnik, U. Rogulis, I. Tale, A. Veispals, *EPR of F-type centres in* $LiBaF_3$, Latvian Journal of Physics and Technical Sciences, **2**, (2004), pp. 62.

[37] U. Rogulis, J.-M. Spaeth, I. Tale, M. Nikl, N. Ichinose, K. Shimamura, *Magnetooptical studies of defects and recombination luminiscence in* $LiBaF_3$, Radiation Measurements, **38**, (2004), pp. 663.

[38] R. Kaplan, P. J. Bray, *Electron-Spin Paramagnetic Resonance Studies of Neutron-Irradiated LiF*, Physical Review, **129**(5), (1963), p. 1919.

Author's publication list

[1*] A. Fedotovs, E. Elsts, U. Rogulis, A. Gulans, I. Tale, M. Nikl, N. Ichinose, K. Shimamura, *EPR hyperfine structure of F-type centres in pure LiBaF*$_3$ *crystal*, Physica Status Solidi (c), **4/3**, (2007), pp. 1284.

[2*] A. Fedotovs, U. Rogulis, L. Dimitrocenko, *Electron paramagnetic resonance studies of radiation defects in LiYF*$_4$ *crystal*, Latvian Journal of Physics and Technical Sciences, **6**, (2006), pp. 60.

[3*] L. Dimitrocenko, U. Rogulis, A. Veispals, M. Springis, P. Kulis, A. Fedotovs, A. Misnev, *Luminscence of Ce-doped borate-oxyfluoride glass ceramics*, Physica Status Solidi (c), **4/3**, (2007), pp. 753.

[4*] A. Fedotovs, L. Dimitrocenko, U. Rogulis, *EPR of radiation defects in LiYF*$_4$ *crystal*, Proceedings of the International Conference on Inorganic Scintillators and their Industrial Applications SCINT2005, **1**, (2006), pp. 162.

[5*] A. Fedotovs, E. Elsts, U. Rogulis, I. Tale, M. Nikl, N. Ichinose, K. Shimamura, *EPR of F type centres in LiBaF*$_3$, Proceedings of the International Conference on Inorganic Scintillators and their Industrial Applications SCINT2005, **1**, (2006), pp. 156.

[6*] A. Fedotovs, U. Rogulis, *Perturbed Cd centre in BaF*$_2$ *crystal*, Latvian Journal of Physics and Technical Sciences, **3**, (2005), pp. 62.

[7*] U. Rogulis, A. Veispals, L. Dimitrocenko, M. Springis, P. Kulis, A. Fedotovs, *Optical properties of Ce-doped oxifluoride composites*, Latvian Journal of Physics and Technical Sciences, **2**, (2006), pp. 111.

Conferences

[1] L. Dimitrocenko, U. Rogulis, A. Veispals, M. Springis, P. Kulis, A. Fedotovs, *Luminiscence of Ce-doped borate-oxyfluoride glass ceramics*, *Abstr. of EURODIM2006, Milano, Italy*, p. 136.

[2] E. Elsts, A. Fedotovs, U. Rogulis, A. Guļāns, I. Tāle, *F-tipa centru EPR LiBaF$_3$ kristālā*, *LU CFI 22. zinātniskās konferences tēzes*, p. 8.

[3] A. Fedotovs, L. Dimitročenko, U. Rogulis, *Radiācijas defektu EPR LiYF$_4$ kristālos*, *LU CFI 22. zinātniskās konferences tēzes*, p. 7.

[4] A. Fedotovs, L. Dimitrocenko, U. and Rogulis, *EPR of radiation defects in LiYF$_4$ crystal*, *Abstr. of SCINT2005, Alushta, Ukraine*, p. 62.

[5] A. Fedotovs, E. Elsts, U. Rogulis, A. Gulans, I. Tale, M. Nikl, N. Ichinose, K. Shimamura, *EPR hyperfine structure of F-type centres in pure LiBaF$_3$ crystal*, *Abstr. of EURODIM2006, Milano, Italy*, p. 340.

[6] A. Fedotovs, E. Elsts, U. Rogulis, I. Tale, M. Nikl, N. Ichinose, K. Shimamura, *EPR of F type centres in LiBaF$_3$*, *Abstr. of SCINT2005, Alushta, Ukraine*, p. 60.

[7] A. Fedotovs, V. Pankratov, L. Grigorjeva, D. Millers, U. Rogulis, *EPR spectra of radiation defects in YVO$_4$ crystals*, *Abstr. of SCINT2007, Winston-Salem, USA*, p. 143.

[8] A. Fedotovs, V. Pankratovs, L. Grigorjeva, D. Millers, U. Rogulis, *Tīru un aktivētu YVO$_4$ kristālu EPR spektri*, *LU CFI 23. zinātniskās konferences tēzes*, p. 38.

[9] A. Fedotovs, U. Rogulis, *Cd piejaukuma defektu EPR BaF$_2$ kristālos*, *LU CFI 19. zinātniskās konferences tēzes*.

[10] A. Fedotovs, U. Rogulis, A. Šarakovskis, L. Dimitročenko, *Radiācijas defektu EPR fluorīdu kristālos un oksifluorīdu stikla keramikā*, *LU CFI 24. zinātniskās konferences tēzes*, p. 16.

[11] A. Fedotovs, U. Rogulis, L. Dimitročenko, *Radiācijas defektu EPR $LiYF_4$ kristālā*, *LU CFI 21. zinātniskās konferences tēzes*, p. 9.

[12] A. Fedotovs, U. Rogulis, L. Dimitrocenko, *EPR of intrinsic defects in $LiYF_4$ crystal*, *Abstr. of SCINT2007, Winston-Salem, USA*, p. 104.

[13] A. Fedotovs, U. Rogulis, L. Dimitrocenko, *Electron paramagnetic resonance studies of radiation defects in $LiYF_4$ crystal*, *Abstr. of LUMDETR2006, Lviv, Ukraine*, p. 190.

[14] A. Fedotovs, U. Rogulis, A. Sarakovskis, L. Dimitrocenko, *EPR of radiation defects in lithium-oxyfluoride glass ceramics*, *Abstr. of ICDIM2008, Aracaju, Brazil*, p. A053.

[15] U. Rogulis, A. Veispāls, L. Dimitročenko, M. Spriņģis, P. Kūlis, A. Fedotovs, *Optical properties of Ce-doped oxyfluoride composites*, *2. Latvijas konferences "Funkcionālie materiāli un nanotehnoloģijas" tēzes, Rīga*, p. 61.

Acknowledgement

I would like to express sincere gratitude to my colleagues at the Institute of Solid State Physics: Uldis Rogulis, Anatolijs Šarakovskis, Māris Spriņğis, Lauris Dimitročenko and Jānis Trokšs for successful collaboration and invaluable help during this work. Also I would like to thank Dzintars, Ilze, Ļena and other my close friends for the support and being together during fun and hard parts of my whole studies. Special thanks goes to the bureau Graf-X, and especially to Ruta Krūskopa, Ilze, Mārtiņš and, of course Dagnija!

This scientific contribution was done with financial support by European Social Fund (ESF).